

**A STUDY OF EJECTION TIMES OF TERRESTRIAL PLANETS
FROM THE HABITABLE ZONES OF THE SOLAR TWINS
HD 20782 AND HD 188015**

by
KATHERINE ELIZABETH YEAGER

Presented to the Faculty of the Graduate School of
The University of Texas at Arlington in Partial Fulfillment
of the Requirements
for the Degree of

MASTER OF SCIENCE IN PHYSICS

THE UNIVERSITY OF TEXAS AT ARLINGTON

August 2009

Copyright © by KATHERINE ELIZABETH YEAGER 2009

All Rights Reserved

Dedicated to my parents, Dave and Carleen Yeager, for always pushing me to reach
my goals and letting me shoot for the stars.

ACKNOWLEDGEMENTS

I would like to thank my supervising professor Dr. Manfred Cuntz for constantly motivating and encouraging me throughout my studies towards a Master's degree. I wish to thank Dr. Zdzislaw Musielak for taking an interest in my research and providing me with insight even though he was not able to serve on my committee. I would also like to thank Dr. Lopez and Dr. Zhang for taking time to serve on my committee.

I would also like to express my deep gratitude to my parents, Dave and Carleen Yeager, without whom I would have never pushed myself to reach my goals. They have motivated me and encouraged me every step of the way. I am also very grateful to my fiancé, Mark, for his constant encouragement and help in any way that he could. Without him, I would have never achieved the high grades in physics that I have. I would also like to thank my siblings Carrie, Keith, and Molly for their perspectives and allowing me to develop mine even if they are completely different from their own.

Finally, I want to acknowledge all of my friends and acquaintances that I have known throughout my education. I would especially like to thank Jason Eberle for his constant help and advice throughout the course of my Master's Thesis.

July 9, 2009

ABSTRACT

A STUDY OF EJECTION TIMES OF TERRESTRIAL PLANETS FROM THE HABITABLE ZONES OF THE SOLAR TWINS HD 20782 AND HD 188015

KATHERINE ELIZABETH YEAGER, M.S.

The University of Texas at Arlington, 2009

Supervising Professor: MANFRED CUNTZ

We provide a detailed statistical study of the ejection of terrestrial planets from the habitable zones of the solar twins HD 20782 and HD 188015. These systems possess a giant planet that crosses into the stellar habitable zone, thus effectively thwarting the possibility of habitable terrestrial planets. In case of HD 188015, the orbit of the giant planet is essentially circular, whereas in case of HD 20782, it is extremely elliptical. As starting positions for the giant planets, we consider both the apogee and perigee position, whereas the starting positions of the terrestrial planets are widely varied. For the giant planets, we consider models based on their minimum masses as well as models where the masses are increased by 30%. Our simulations indicate a large range of statistical properties concerning the ejection of the terrestrial planets from the stellar habitable zones. For example, it is found that the ejection times for the terrestrial planets from the habitable zones of HD 20782 and HD 188015, originally placed at the center of the habitable zones, vary by a factor of ~ 200 and ~ 1500 , respectively, depending on the starting positions of the giant and terrestrial planets. If the mass of the giant planet is increased by 30%, the variation in ejection

time for HD 188015 increases to a factor of ~ 6000 . As a further application of this thesis we challenge the customary assumption that the entering of a terrestrial planet into the Hill radius (or multiples of the Hill radius) of a giant planet is a valid criterion for its ejection from the star-planet system. This assumption has been widely used in previous studies, especially those with an astrobiological focus. It has been found from our study that even though the terrestrial planets are eventually ejected from the habitable zones of both systems, the “Hill Radius Criterion” is identified as invalid for the prediction of when the ejection is actually occurring.

TABLE OF CONTENTS

ACKNOWLEDGEMENTS	iv
ABSTRACT	v
LIST OF FIGURES	ix
LIST OF TABLES	xi
Chapter	Page
1. INTRODUCTION	1
1.1 Background	1
1.2 Habitable Zone	2
1.3 Orbital Stability	5
1.4 Previous Studies Aimed at the Statistics of Planetary Ejections . . .	9
1.5 The Star-Planet Systems HD 20782 and HD 188015	11
2. THEORETICAL APPROACH (METHOD)	18
2.1 The Three-body Problem	18
2.2 Description of the Program	20
2.3 Test of Accuracy of the Code	23
3. RESULTS AND DISCUSSION	27
3.1 Case Study of HD 20782	27
3.2 Case Study of HD 188015	35
3.3 Statistics of Terrestrial Planet Ejections	42
3.3.1 Analysis of Standard Deviation, Median and Variance	42
3.3.2 Analysis of Skewness and Excess Kurtosis	43
4. FURTHER APPLICATION	52

4.1 The Hill Radius criterion and its validity	52
5. CONCLUSIONS	59
APPENDIX	
A. THE CODE	64
REFERENCES	91
BIOGRAPHICAL STATEMENT	94

LIST OF FIGURES

Figure	Page
1.1 Habitable zone ranges based on spectral type	4
1.2 Mass distribution of extra solar planets	6
1.3 Orbital eccentricities vs. semimajor axis	7
1.4 Distribution of semimajor axes of exoplanets.	8
1.5 Results for the star-planet system HD 2102277	11
1.6 Results for the star-planet system HD 2102277 for various starting positions	12
1.7 Measured velocity vs. time for HD 20782	13
1.8 Measured velocity vs. time for HD 188015	14
1.9 Orbits of the giant planets for HD 188015 and HD 20782.	15
1.10 Locations of $\delta = 0.1$, $\delta = 0.5$, and $\delta = 0.9$ within the HZ.	16
2.1 Case studies for a terrestrial planet	22
2.2 Case studies for a terrestrial planet and terrestrial planet with increased mass of giant planet.	23
2.3 Examples of timestep testing for HD 20782.	25
2.4 Examples of timestep testing for HD 188015.	26
3.1 Ejection times for the star system HD 20782	29
3.2 Case studies of HD 20782 $\delta = 0.1$	32
3.3 Case studies of HD 20782 $\delta = 0.5$	33
3.4 Case studies of HD 20782 $\delta = 0.9$	34
3.5 Ejection times for the star system HD 188015.	36
3.6 Case studies of HD 188015 $\delta = 0.1$	39

3.7	Case studies of HD 188015 $\delta = 0.5$	40
3.8	Case studies of HD 188015 $\delta = 0.9$	41
3.9	Skew and Kurtosis results from Fatuzzo et al.(2006)	49
4.1	Histograms for the ejection of the terrestrial planet from the HZ of HD 20782.	57
4.2	Histograms for the ejection of the terrestrial planet from the HZ of HD 188015.	58

LIST OF TABLES

Table		Page
1.1	Stellar and Planetary Parameters	14
2.1	Tests of computer code for HD 20782	24
2.2	Tests of computer code of HD 188015	24
3.1	Ejection Times $T_{\text{Ej}}^{\text{mean}}$ for HD 20782	45
3.2	Ejection Times $T_{\text{Ej}}^{\text{mean}}$ for HD 188015	46
3.3	Statistical Properties of Ejection Times for HD 20782	49
3.4	Statistical Properties of Ejection Times for HD 188015	50
3.5	Minimum and Maximum Ejection Times T_{Ej} for the star-planet systems HD 20782 and HD 188015	51
4.1	Statistics of R_{H} Ejections	58

CHAPTER 1

INTRODUCTION

1.1 Background

The search for life in the universe is not a new concept. Over the last one and a half decades, the observation, study and characterization of extrasolar planets have become a vibrant field of astrophysical research, resulting in an extraordinary array of discoveries (e.g., Marcy & Butler 1998; Marcy et al. 2005; Jones 2008). A crucial part of this type of research is the determination of the orbital properties of extrasolar planets, which indicates massive planets with many of them located very close to their host stars or having highly eccentric orbits; see, e.g., catalogue by Butler et al. (2006) and subsequent papers. Besides the study of physical properties of extrasolar planets, an important objective of these investigations concern the identification of terrestrial planets in stellar habitable zones (HZs); see, e.g., Gehman et al. (1996), Jones et al. (2001), Noble et al. (2002), and Asghari et al. (2004). These studies are highly relevant in the view of current and future space missions such as *COROT*, *Kepler*, *SIM PlanetQuest*, *Terrestrial Planet Finder [TPF]*, and *Darwin*, which were chiefly designed to detect and explore Earth-type planets around other stars (see Baglin 2003; Borucki et al. 2003; Catanzarite et al. 2006; Borucki et al. 2007; Cockell et al. 2009; Unwin et al. 2008, for detailed information).

To gauge the possibility of habitable terrestrial planets in observed extrasolar planetary systems, as well as theoretical star-planet systems, numerous studies have been undertaken (e.g., Cuntz et al. 2003; von Bloh et al. 2003; 2007) with focus both on the requirement of planetary orbital stability and preliminary descriptions

of the planetary climatology. Both efforts are required to obtain insight into the planetary astrobiological suitability for the existence and evolution of life; see Spiegel et al. (2008) for recent models on extrasolar habitable climates. A statistical analysis indicates that in about 15% to 40% of systems with observed giant planets the orbital stability of hypothetical Earth-mass planets in the stellar HZs would be affected by the giant planet(s) with the exact number depending on the assumed extents of the HZs (see Chapter 3). Catalogues of nearby stellar systems that are expected to fulfill basic preconditions of habitability have been given by, e.g., Turnbull & Tarter (2003) and Sándor et al. (2007).

1.2 Habitable Zone

Surrounding every star there is a region of space where life, given the right circumstances, has possibility of forming. This region is called the Habitable Zone (HZ). The HZ is a region of space where conditions are favorable for life as it may be found on Earth (von Bloh et al. 2003). The HZ is an imaginary spherical shell of space surrounding a star in which the surface temperatures of any planet present might be conducive to the origin and development of life as we know it. For life to exist the surface temperature of the planet must be in the temperature range for liquid water to be present. Water will remain liquid under a pressure of 1 bar (terrestrial sea level pressure) between 0°C and 100°C. There are some extreme cases, however, where life can survive outside these temperature ranges. One such case is on our own planet in Antarctica where temperatures can reach as low as -70°C. The HZ for our own Solar System currently extends from 0.84 AU to an outer limit between 1.37 and 1.67 AU as determined by Kasting et al. (1993). The distance of 1.37 AU marks the point of first CO₂ condensation while the limit of 1.67 AU defines the maximum greenhouse limit on the outer edge of the the HZ. The hot inner edge of a HZ is located at the orbital

distance where a planet's water is broken up by stellar radiation into oxygen and hydrogen. The outer edge of the HZ is determined to be where atmospheric carbon dioxide condenses to eliminate the greenhouse warming effect. For the purposes of this thesis we use the outer limit of 1.67 AU for our HZ limit. The inner and outer limits of the HZ are computed as

$$R_{in} = \left(\frac{L}{L_{\odot} \cdot S_{in}(T_{\text{eff}})} \right)^{\frac{1}{2}} \quad (1.1)$$

$$R_{out} = \left(\frac{L}{L_{\odot} \cdot S_{out}(T_{\text{eff}})} \right)^{\frac{1}{2}} \quad (1.2)$$

with L and L_{\odot} as stellar and solar luminosity, respectively, and T_{eff} as stellar effective temperature. Moreover, $S_{in}(T_{\text{eff}})$ and $S_{out}(T_{\text{eff}})$ are second order polynomials depicting the stellar flux at the inner and outer boundaries of both the conservative and general HZ as have been given by Underwood et al. (2003). Since we are using the same inner and outer limits for the HZ as Kasting et al. (1993) and Underwood et al. (2003), T_{eff} is taken to be 5778 ± 3 K for the Sun (Stix 2004). The planet existing within the HZ would have to be rocky, of the same order as the Earth's mass, and would had to lie in an orbit within the HZ for at least the order of a billion years for life to have had a detectable effect on its atmosphere (Underwood et al. 2003).

HZs are not only determined based on temperature of the star, they are also determined based on the type of star. There are seven different star types on the main sequence (O B A F G K M) but only five of them are generally used when determining a HZ. In general, hot, luminous stars all have wide HZs, with inner margins located relatively far out from the star (Kasting et al. 1993). The two types of stars that are generally not considered when looking for planets within HZs are the O and B type stars. These stars have extremely short lifetime compared to the

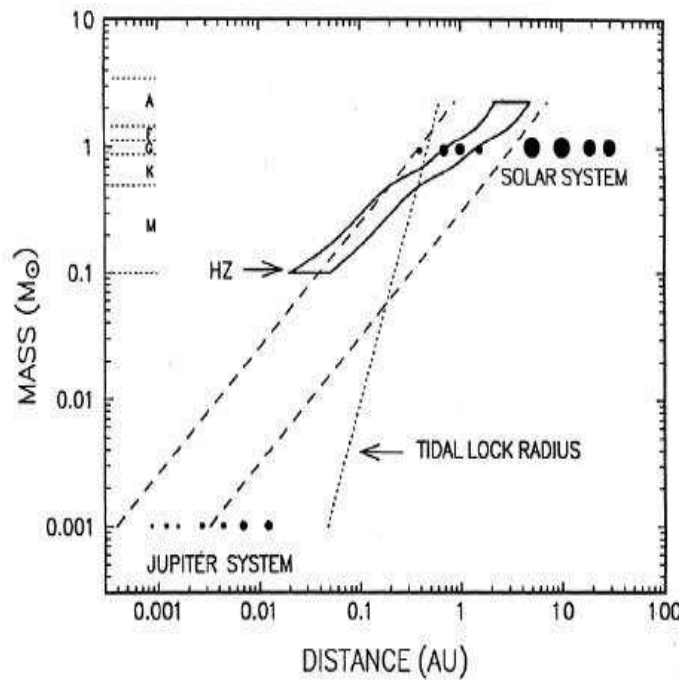


Figure 1.1. Habitable Zone Ranges Based on Spectral Type. Credit: Franck et al. (2002).

smaller and dimmer stars, ranging only a few tens of millions of years which is not nearly long enough for even primitive life to form. Another concern with O and B type stars is the amount of UV radiation that is emitted from these stars. These two star types emit an amount of UV radiation that would surely destroy any life that could possibly form on these planets. As for the other five star types, the amount of UV radiation emitted is within the range that could help with the formation of important atmospheric dynamics such as the formation of ozone. The habitable zone around these five star types range in size and distance from the star based on the spectral type of the star (Kasting et al. 1993). Figure 1.1 shows how the width and distance of the HZ from the star varies with spectral type.

The HZ evolves during a star's main sequence lifetime - the boundaries generally migrate outwards. During this time, nuclear burning of hydrogen builds up a helium

residue in a stellar core causing an increase in pressure and temperature. This occurs more rapidly in stars that are more massive and lower in metallicity. These changes are transmitted to the outer regions of a star, which results in a steady increase in luminosity and changes in effective temperature. The major effect is that a star becomes more luminous, causing HZ to move outwards (Underwood et al. 2003).

The HZ around various stars gives us an approximate idea as to where we should spend our time looking for the possibility of life in the Universe. A planet lying within the HZ is only the first criterion for life as we know it. The next criterion that we must consider is the amount of time a planet spends within the HZ of the star, otherwise known as the orbital stability of the planet. For the purpose of this thesis we will examine the orbital stability for the terrestrial planet for two extreme cases, one with a fairly circular orbit and the other for a highly elliptical orbit.

1.3 Orbital Stability

Planetary habitability requires orbital stability of the Earth-type planet over a biologically significant length of time in the HZ. The analysis of orbital stability of hypothetical terrestrial planets in extrasolar planetary systems has to take into account the effects of the giant planet(s) in those systems. In many cases the giant planet restricts the orbital stability of the terrestrial planet to a small or very small orbital domain or prevent orbital stability completely (von Bloh et al. 2003).

To date (July 1, 2009), <http://exoplanet.eu>, lists a total number of 278 exoplanetary systems discovered with a total of 353 extrasolar planets. Out of these 353 planets a vast majority (on the order of 336) have a semimajor axis of less than 10 AU, and in most cases are less than 1 AU (to date 192 planets). Most of these planets have been discovered by observing cyclic Doppler shifts in the stellar spectral lines. This gives $m \cdot \sin(i_o)$, where m is the mass of the planet and (i_o) is the inclination of

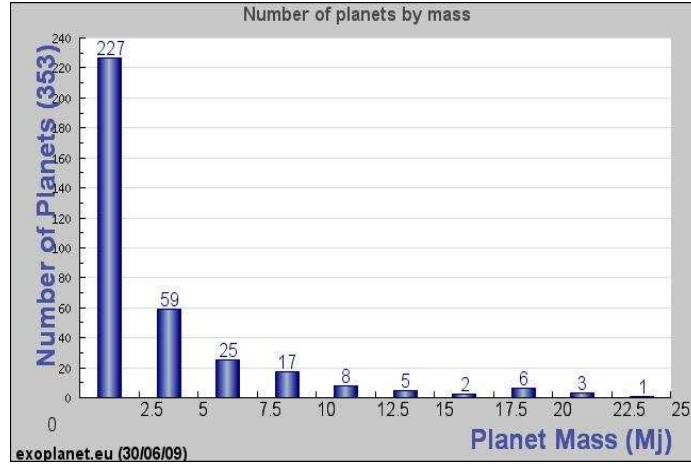


Figure 1.2. Mass distribution of extra solar planets.

the orbital plane of the planet with respect to the plane of the sky (Jones et al. 2001). Values of $m \cdot \sin(i_o)$ range from $7 \cdot 10^{-5} M_J$ (PSR 1257+12b) to $21.66 M_J$ (CoRoT 3b), where M_J is the mass of Jupiter. The likelihood of objects that exceed $13 m_J$ being brown dwarfs and not actual planets is quite high. The planet PSR 1257+12b orbits a pulsar and thus does not have the possibility of harboring life. The majority of planets that have been detected have masses in the range of $2 \cdot 10^{-2}$ to $5 m_J$. As our technology improves we are slowly being able to detect planets with masses much closer to our own planet.

The majority of planets detected have been found using the radial velocity detection method. This method is used by carrying out a series of observations of the spectrum of light emitted by a star. Periodic variations in the star's spectrum may be detected, with the wavelength of characteristic spectral lines in the spectrum increasing and decreasing regularly over a period of time. These variations may be indicative of the radial velocity of the star being altered by the presence of a planet orbiting the star, causing Doppler shifts in the light emitted by the star. If an extrasolar planet is detected, its mass can be determined from the changes in the

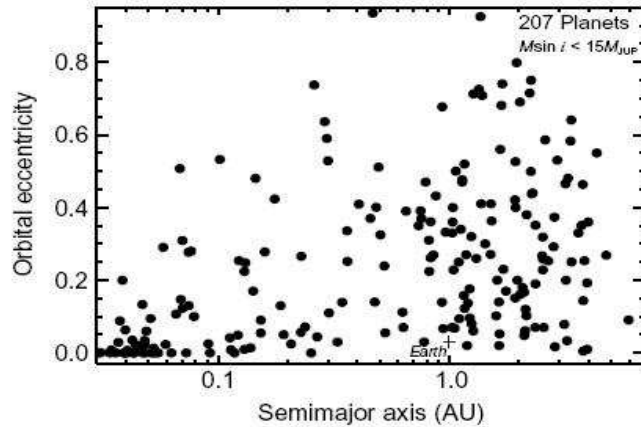


Figure 1.3. Orbital eccentricities versus semimajor axis (on a log scale) of the extra-solar planets detected to date in March of 2008. Credit: Marcy et al. (2008).

star's radial velocity. A graph of measured radial velocity versus time will give a characteristic curve (sine curve in the case of a circular orbit), and the amplitude of the curve will allow the planet's mass to be calculated. Due to the nature of this method, it is much easier to detect planets of much higher mass than that of our own planet (Schneider 2009). Currently to date the lowest mass planet found is approximately 1.9 Earth masses. This is the first of Earth mass type planets found. Several supermassive terrestrial planets, or Super-Earths, have also been discovered, but these planets are typically on the order of 2 to 10 times the mass of the Earth. Unfortunately none of these Earth type planets have been found to reside within its host star's HZ.

Another limitation of this method is that it is bias to exoplanets with a low eccentricity and small semimajor axis. This is due to the fact that it takes much less time to determine the periodic variations in the star's spectrum if the planet is very close to the star. A high eccentricity requires a longer sample period of the star to determine if the variations are indeed a planet. An example of this bias in exoplanet eccentricity and semimajor axis can be seen in (Figs. 1.3 and 1.4).

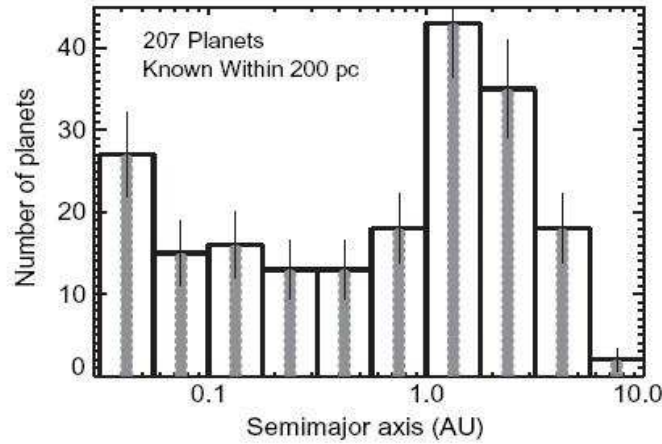


Figure 1.4. Distribution of semimajor axes of exoplanets. Credit: Marcy et al. (2008).

On March 4, 2009 the Kepler mission was launched which should allow us to discover more Earth-type planets. It has a much higher probability of detecting Earth-like planets than the Hubble Space Telescope, since it has a much larger field of view and will be dedicated to detecting planetary transits. The Hubble Space Telescope in contrast focused on just one starfield, while the Kepler Mission is designed to observe 100,000 stars simultaneously. This means that Kepler is much more likely to discover an Earth-like planet. The Kepler Mission is specifically designed to survey our region of the Milky Way galaxy to discover hundreds of Earth-size and smaller planets in or near the HZ and determine how many of the billions of stars in our galaxy have such planets (Koch & Gould 2009).

When a planet crosses in front of its star as viewed by an observer, the event is called a transit. Transits by terrestrial planets produce a small change in a star's brightness of about $1/10,000$ lasting for 2 to 16 hours. This change must be absolutely periodic if it is caused by a planet. In addition, all transits produced by the same planet must be of the same change in brightness and last the same amount of time, thus providing a highly repeatable signal and robust detection method. Once

detected, the planet's orbital size can be calculated from the period and the mass of the star using Kepler's Third Law of planetary motion. The size of the planet is found from the depth of the transit (amount of decrease in luminosity) and the size of the star. From the orbital size and the temperature of the star, the planet's characteristic temperature can be calculated. From this, the question of whether or not the planet is habitable can be answered. Using the transit technique should yield us with more precise information about the mass and size of the host stars and the extrasolar planets.

1.4 Previous Studies Aimed at the Statistics of Planetary Ejections

Previous studies of this type of research have been carried out but not to the degree that we will look at in further chapters of this thesis. It is worth mentioning some of the limitations and findings of the previous studies.

Jones et al. (2001) studied the orbital stability of six extrasolar planets, all of which have an eccentricity of less 0.3 with the exception of one exoplanet with an eccentricity of 0.41 which resides in a star planet system with two other giant planets. The authors use a second-order mixed-variable symplectic (MVS) integrator. One main downside to using this type of integrator, however, is that MVS integrators cannot handle close encounters between planets accurately, because the part of the Hamiltonian that describes the planetary interactions is then comparable with the star-planet Hamiltonian. The smallest distance at which it is safe to use the integrator is about three times the Hill Radius of the planet in the encounter with the larger Hill Radius. The Hill Radius refers to the gravitational sphere of influence of one astronomical body such as Earth in the presence of perturbations from another heavier body (Sun) around which it orbits. According to Jones et al. (2001), when the two planets are separated by the Hill Radius, their gravitational interaction is of

the same order as the gravitational interaction of each planet with the star, and so considerable orbital modification will occur, particularly for the terrestrial planet in a giant-terrestrial encounter. The authors then halt the integration at 3 times the Hill Radius, which not only avoids using the MVS integrator in an inaccurate domain, it is also a conservative definition of the point at which orbits become unstable (Jones et al. 2001). We will discuss the significance of this statement in later chapters of this thesis.

Noble et al. (2002) studied the orbital stability of three star-planet systems, which overall amount to four extrasolar planets. The authors use a fourth-order Runge-Kutta integration scheme, which consequently is extremely similar to the integration scheme used for the simulations carried out in this thesis. The benefit of using this integration scheme is that it can handle close encounters between planets, whereas the previous method discussed cannot. We will discuss the fourth-order Runge-Kutta integration scheme in later chapters of this thesis. It is important, however, to mention that the results obtained by Noble et al. (2002) for the star-planets system of HD 210277 are extremely similar to the results obtained in this thesis. The following figures represent the results obtained from Noble et al. (2002) for the star-planet system HD 210277. It can be seen from these figures (Figs. 1.5 and 1.6) that these planets slowly migrate out of the HZ over time, thus rendering the planet uninhabitable.

The final study that we would like to discuss is that of Fatuzzo et al. (2006). This work is for that of the statistical stability analysis around binary stars. Even though our work is for that of a single star system, it is worth noting that the results found from this study carried out by Fatuzzo et al. (2006) very much mirrors our own results for the single star system. We will discuss this work much more extensively in chapter 3 of this thesis.

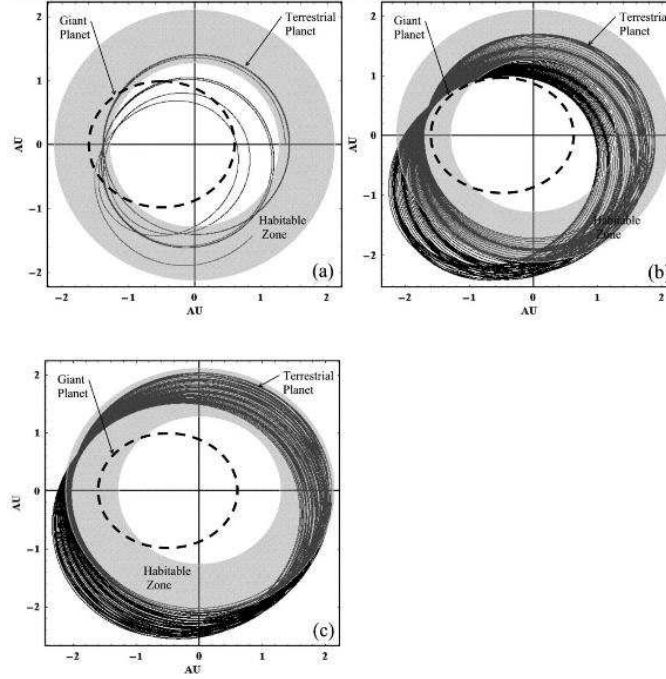


Figure 1.5. Results for the star-planet system HD 2102277 for $\theta = 0^\circ$ but $\delta = 0.1$, $\delta = 0.5$, & $\delta = 0.9$ respectively. Credit: Noble et al. (2002).

1.5 The Star-Planet Systems HD 20782 and HD 188015

For our study we selected the two star-planet systems HD 20782 and HD 188015. Each system contains a Jupiter-type planet with a minimum mass of 1.78 and $1.50 M_J$, respectively (Butler et al. 2006); see Table 1.1 for information on the adopted stellar and planetary parameters with all symbols having their usual meaning. Furthermore, the central stars of the two systems are very similar to our Sun. The masses of the two stars are 0.98 ± 0.05 and $1.09 \pm 0.05 M_\odot$ and the stellar effective temperatures are 5758 ± 44 and 5746 ± 44 K, respectively (Butler et al. 2006). Since the effective temperatures and luminosities of HD 20782 and HD 188015 agree with the Sun within the error bars, and both stars are G type stars, we are entitled to assume that the HZs of the two stars are identical to the HZ of the Sun. Therefore, following Kasting

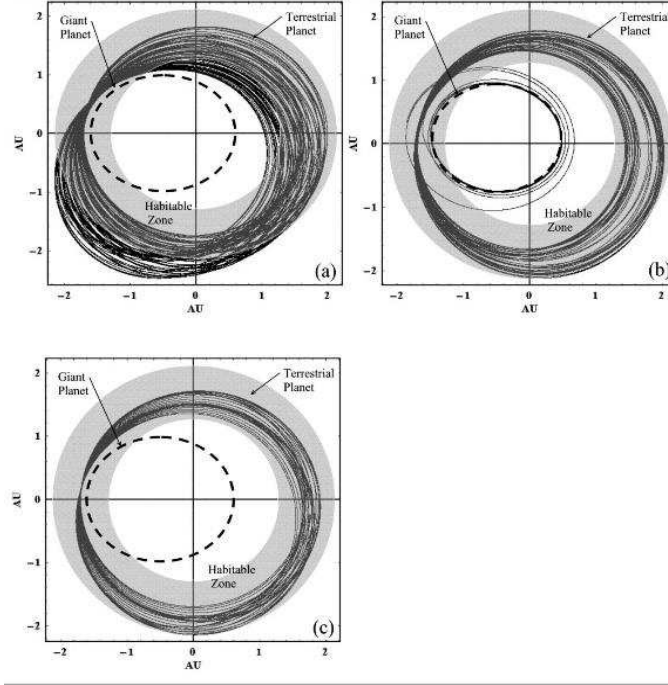


Figure 1.6. Results for the star-planet system HD 2102277 for $\delta = 0.5$ but with $\theta = 0^\circ$, 120° , & 180° respectively. Credit: Noble et al. (2002).

et al. (1993), the inner and outer edges of the HZs are assumed to be located at 0.84 and 1.67 AU, as previously mentioned, from the star.

Both star systems were discovered using Doppler measurements (the radial velocity method) which was outlined in the previous section. In the case of HD 188015 an iodine technique was used. This technique is outlined in Marcy et al. (2005). Measurements were taken of both star systems allowing the observers to fit the data to a best-fit Keplerian model which include internal errors of the detection technique as well as the jitter of the star (see Marcy et al. 2005; Jones et al. 2006, for detailed information). From the Keplerian curve the orbital period, as well as velocity amplitude and eccentricity of the planet may be determined. All of the necessary values obtained from the studies of these two star systems are shown in Table 1.1. The fol-

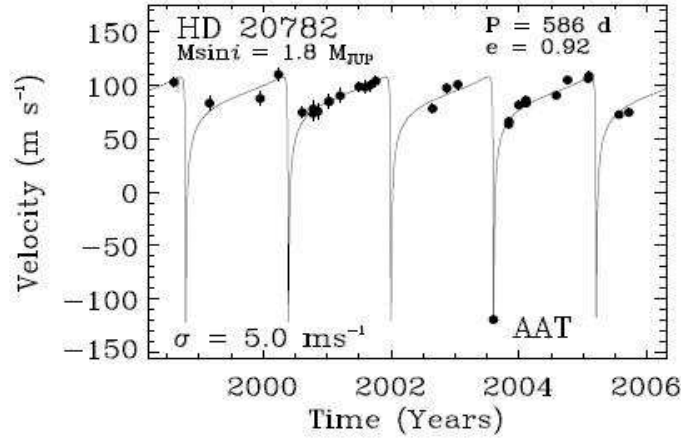


Figure 1.7. Measured velocity vs. time for HD 20782 (dots) with the associated best-fit Keplerian. Credit: Jones et al. (2006).

lowing figures (Figs. 1.7 and 1.8) show the the velocity vs time plots with the doppler velocities obtained from the measurements as well as the best-fitting Keplerian.

The two star-planet systems HD 20782 and HD 188015 are radically different compared to the solar case. In these systems the giant planet either remains in or crosses into the stellar HZs, thus effectively thwarting the possibility of habitable Earth-type planets; see Noble et al. (2002) for previous simulations of HD 210277 also showing this type of outcome. In case of HD 188015, the orbit of the giant planet is essentially circular, with a perigee and apogee of 1.04 and 1.37 AU, where $r_{\max} = a(1 + e)$ and $r_{\min} = a(1 - e)$ respectively, both located in the stellar HZ (see Fig.1.9). On the other hand, the orbit of the giant planet in the system of HD 20782 is extremely elliptical, noting that its perigee is at 0.10 AU and its apogee is at 2.63 AU. The variations in these two orbits can be seen in Fig. 1.9. The interactions between an terrestrial planet placed at various distances within the HZ and the Extra-Solar Giant Planet (EGP) corresponding with the designated star system will be looked at in detail through the remainder of this thesis. We will show how the EGP affects the

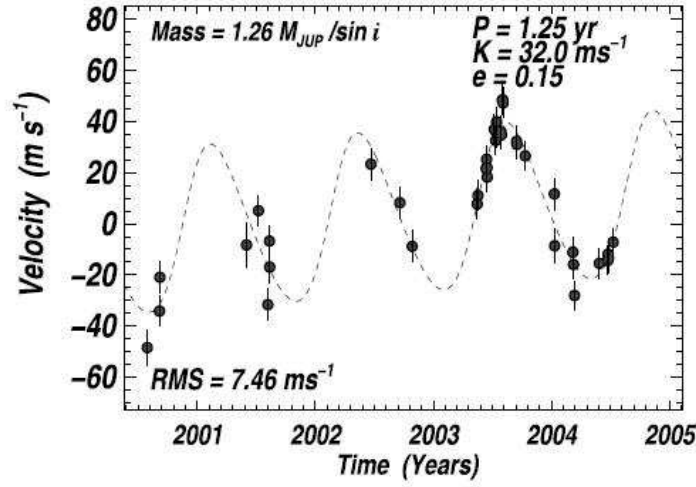


Figure 1.8. Measured velocity vs. time for HD 188015 (dots) with the associated best-fit Keplerian. Credit: Marcy et al. (2005).

Table 1.1. Stellar and Planetary Parameters

Parameter	HD 20782	HD 188015
T_{eff} (K)	5758 ± 44	5746 ± 44
M_{\star} (M_{\odot})	0.98 ± 0.05	1.09 ± 0.05
R_{\star} (R_{\odot})	1.10 ± 0.10	1.04 ± 0.10
Distance (pc)	36.0 ± 1.1	52.6 ± 2.6
[Fe/H]	-0.051 ± 0.030	0.289 ± 0.030
a_p (AU)	1.364 ± 0.079	1.203 ± 0.070
e_p	0.925 ± 0.030	0.137 ± 0.026
P (days)	585.86 ± 0.03	461.2 ± 1.7
$m_p \sin i$ (M_J)	1.78 ± 0.34	1.50 ± 0.13

Note. — Data given by Butler (2006) and references therein, notably Valenti and Fischer (2005).

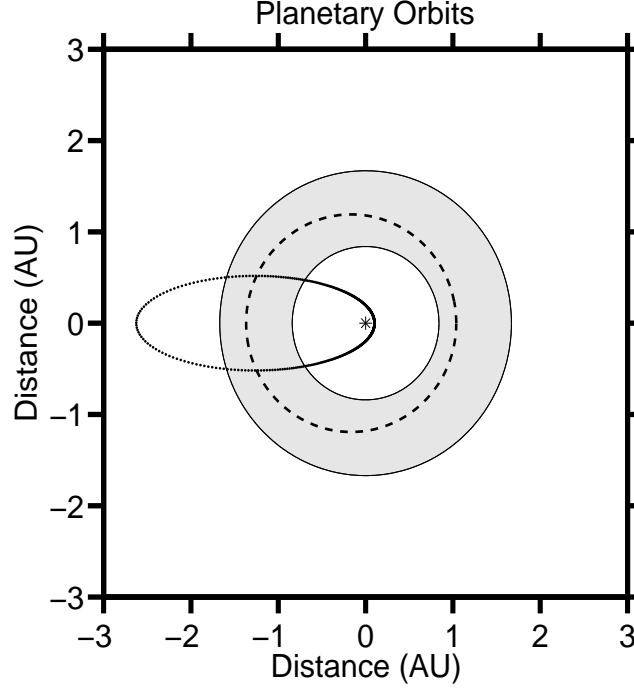


Figure 1.9. Orbits of the giant planets for the two represented systems, which are HD 188015 (*dashed line*) and HD 20782 (*narrow dotted line*). We also give the HZs (*gray area*) for the two systems. The two HZs are assumed to have identical extents.

orbital stability of the terrestrial planet. It should also be noted that at this time these two systems only consist of a star and a giant planet and that no other planets have been detected within the system.

Each star system was tested using only slight changes in the starting position of the terrestrial planet. For this study, the terrestrial planet was placed at three different initial starting positions within the HZ. These distances are defined as $\delta = 0.1$, $\delta = 0.5$, and $\delta = 0.9$, where $\delta = 0.1$ is located towards the inner edge of the HZ, $\delta = 0.5$ is in the middle of the HZ, and $\delta = 0.9$ is near the outer edge of the HZ. Figure 1.10 illustrates the locations of each of these positions.

Each simulation also varied by changing the starting position of the terrestrial planet between 0° and 350° in 10° increments. Throughout each set of simulations

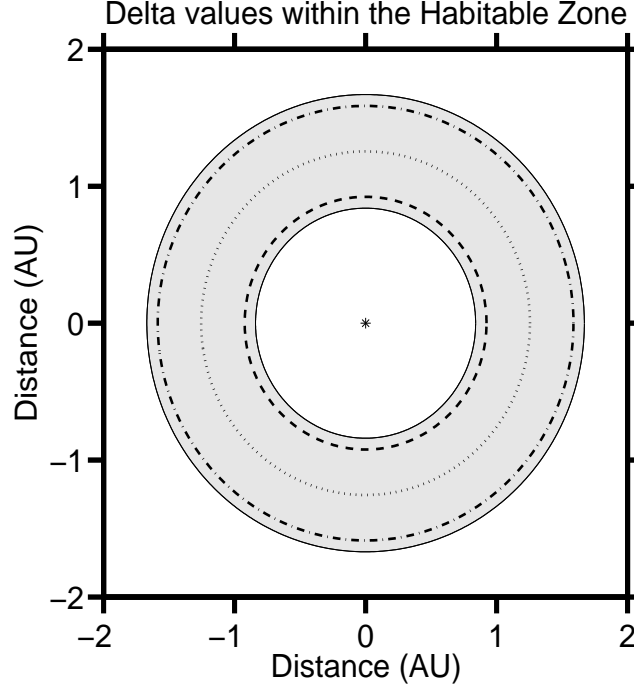


Figure 1.10. Locations of $\delta = 0.1$, $\delta = 0.5$, and $\delta = 0.9$ within the HZ. $\delta = 0.1$ is located near the inner edge of the HZ, $\delta = 0.5$ is located in the middle of the HZ, and $\delta = 0.9$ is located near the outer edge of the HZ .

the giant planet was designated to start at either apogee or perigee depending on the case being studied. Each of the giant planets were detected using the radial velocity method. Therefore as another case of the study we also used an increased mass of the giant planet of $1.3 \cdot m \cdot \sin(i_o)$ for the two cases of $\delta = 0.5$ for apogee and perigee of both star systems. The factor of 1.3 is motivated by the theoretical result that in the absence of detailed information on the inclination term $\sin i$ the appropriate default term is $\pi/4$ (Gray 1992), corresponding to a factor of 1.273 for the planet mass increase.

In the following chapters we will discuss in detail our theoretical approach. We will discuss the adopted methods and the system parameters concerning HD 20782 and HD 188015. Thereafter, we will describe our results including our findings about

the statistical properties of planetary ejections as well as selected examples of simulations for HD 20782 and HD 188015 with different starting conditions for the giant and Earth-mass planets. Finally, we will present our conclusions.

CHAPTER 2

THEORETICAL APPROACH (METHOD)

2.1 The Three-body Problem

The general setup of our work is for that of the Three-body problem. The system set-up being a star at the center and two planets orbiting that star. The program that was developed to test this set up is dependent on the initial conditions of the star and the two planets. We are assuming that all three bodies lie within the same orbital plane therefore $\dot{\phi} = 0$. The position is easy to determine due to the fact that we choose the starting distance and angle, but the calculation of the velocities of the giant planet and the terrestrial planet are not nearly as straight forward. The following derivation for the velocity equation loosely follows derivations listed in Fowles & Cassiday (2005) and Carroll & Ostlie (2006).

For an elliptic orbit, the square of the speed is given in polar coordinates as

$$v^2 = \dot{r}^2 + r^2\dot{\theta}^2 \quad (2.1)$$

using

$$r\dot{\theta} = \frac{l}{\mu r} = \frac{l}{\mu p}(1 + e \cdot \cos \theta) \quad (2.2)$$

and

$$\dot{r} = \frac{p \cdot e \cdot \sin \theta}{(1 + e \cdot \cos \theta)^2} \cdot \dot{\theta} = \frac{p \cdot e \cdot \sin \theta}{(1 + e \cdot \cos \theta)^2} \cdot \frac{l}{\mu r^2} \quad (2.3)$$

or

$$\dot{r} = \frac{p \cdot e \cdot \sin \theta}{(1 + e \cdot \cos \theta)^2} \cdot \frac{l}{p^2 \mu} \cdot (1 + e \cdot \cos \theta)^2 = \frac{le}{p\mu} \sin \theta. \quad (2.4)$$

where r is the distance between the star and the planet, θ is the angle between the axis and the planet, a is the semimajor axis, e is the eccentricity, p is the latus rectum, μ is the reduced mass, and $l = \mu r^2 \dot{\theta} = \text{constant}$.

We then obtain

$$v^2 = \left(\frac{le}{p\mu} \right)^2 \sin^2 \theta + \left(\frac{l}{\mu p} \right)^2 \cdot (1 + e \cdot \cos \theta)^2 \quad (2.5)$$

After some algebra and noting that $(1 + e \cdot \cos \theta) = p/r$, $(1 - e^2) = p/a$, and $p = l^2/\mu k$ we end up with

$$v^2 = \frac{k}{\mu} \left(\frac{2}{r} - \frac{1}{a} \right). \quad (2.6)$$

We may now simplify this further by noting that $r = a(1 - e)$ when the planet is at perigee. Substituting this value in for r we obtain

$$v^2 = \frac{k}{\mu} \left(\frac{2}{a(1 - e)} - \frac{1}{a} \right), \quad (2.7)$$

which further simplifies to

$$v^2 = \frac{k}{\mu a} \frac{1 + e}{1 - e}. \quad (2.8)$$

Now it is useful for us to simplify μ/k .

$$\mu = \frac{m \cdot M}{m + M} \quad (2.9)$$

and

$$k = GmM \quad (2.10)$$

where M is the larger mass, m is the smaller mass, and G is the gravitational constant.

Since $m \ll M$ we can simplify

$$\frac{\mu}{k} = \frac{mM}{m + M} \frac{1}{GmM} = \frac{1}{G(m + M)} \approx \frac{1}{GM} \quad (2.11)$$

which results in

$$v = \sqrt{\frac{GM}{a}} \sqrt{\frac{1 + e}{1 - e}}. \quad (2.12)$$

Using Kepler’s third law

$$T^2 = \frac{4(\pi)^2 \mu}{k} a^3 \quad (2.13)$$

which then simplifies to

$$T = 2\pi a \sqrt{\frac{a}{GM}} \quad (2.14)$$

and then rearranged to yield

$$\sqrt{\frac{GM}{a}} = \frac{2\pi a}{T}. \quad (2.15)$$

we are then able to substitute this information into Eq. (2.12) and finally obtain

$$v = \frac{2\pi a}{T} \sqrt{\frac{1+e}{1-e}}. \quad (2.16)$$

This is the result used to determine the initial conditions for the velocities of both the giant and terrestrial planets. It should also be noted that the terrestrial planet starts in a circular orbit and therefore has an eccentricity of zero.

2.2 Description of the Program

For each of our simulations, we consider both the observed giant planet and a hypothetical terrestrial planet of one Earth-mass, i.e., $3.005 \times 10^{-6} M_{\odot}$, to execute a grid of model computations. The method of integration assumes a fourth-order Runge-Kutta integration scheme (Press et al. 1989). The code has extensively been tested against known analytical solutions, including two-body and restricted three-body problems (see Noble et al. 2002; Cuntz et al. 2007; Eberle et al. 2008, for detailed results). In the particular framework of our simulations, which are limited to about 10^3 yrs due to the ejection of the terrestrial (Earth-mass) planet from the system, we found that a precision of 10^{-4} for the integration scheme is perfectly sufficient. We arrived at this value by performing detailed test simulations while comparing the ejection times for Earth-mass planet.

For each star system several different cases were studied. The main goal of this thesis was to determine the orbital stability effects when the Earth-mass planet is placed at different initial positions. To begin each set of simulation runs the Earth-mass planet was placed at either $\delta = 0.1$, $\delta = 0.5$ or $\delta = 0.9$ within the HZ for a given starting position of the giant planet (perigee or apogee). We then proceeded to change the starting position of the Earth-mass planet in 10° increments ranging from 0° to 350° with 0° corresponding to the perigee of the giant planet, resulting in 36 simulations. The same process was carried out for each possible combination of starting positions, resulting in six data sets for each star. The initial conditions for the Earth-mass planet were taken to be the initial position in the x and y direction and then calculating the initial velocity in both of these directions as well. For simplicity we are taking all of these calculations to be in the same plane as the giant planet and the host star and therefore allowing the z axis position and velocity to be 0.

The giant planet was taken to always start at either apogee or perigee. This suggests that there is no y axis coordinate for the giant planet and no x axis velocity for the initial conditions of the giant planet. The host star, for simplistic reasons, is considered to be starting at rest, but the program takes this into account and is adjusted to conserve angular momentum. Once the program is started, all three bodies begin to interact with each other. As one would expect, the orbit of the Earth-mass planet is almost immediately heavily disturbed by the gravitational pull of the giant planet, leading to a more elliptical orbit and ultimately to its ejection from the HZ within 10^{-2} to 10^3 yrs. We also find that small changes in the starting position of the Earth-mass planet often result in extremely different outcomes and ejections time. This behavior is well visible in Fig. 2.1 depicting two case studies of orbits for an Earth-mass planet in the star-planet system of HD 188015. In both models, the giant planet was initially placed at perigee, whereas the starting positions of the

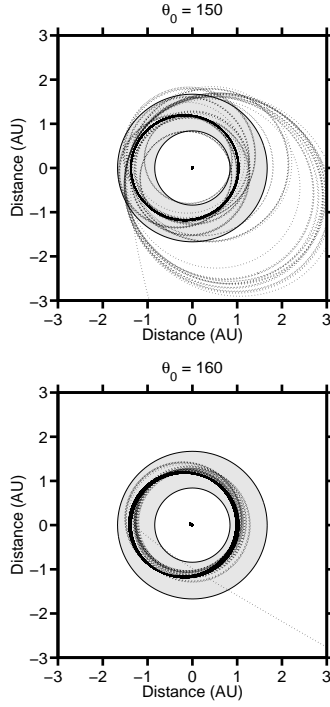


Figure 2.1. Case studies of orbits for a terrestrial planet (dotted line) in HZ (gray area) of HD 188015 based on a simulation time of 1000 years. Note that in both models, the giant planet (solid line) is initially placed at perigee. The starting positions of the Earth-mass planets are given as $\delta = 0.5$ at an angle of 150° and 160° , respectively.

Earth-mass planet were at an angle of 150° and 160° , respectively. At this point it is useful to note that the unit of time will be the AU year (the period of a circular orbit of radius 1 AU). In these units, the product $GM = 4\pi^2 a^3 / T^2$ with a in [AU] and T in [yr].

We also produced another set of simulations where the masses of the giant planets for HD 20782 and HD 188015, with a minimum mass of 1.78 and 1.50 M_J (Butler et al. 2006), respectively, were increased by a factor of 1.3. This result was studied because we do not know the exact value of $\sin(i)$. The simulations were run again for this new mass value for the cases of $\delta = 0.5$ for both the apogee and perigee positions of the giant planet. We then compared the effects of the new mass on the

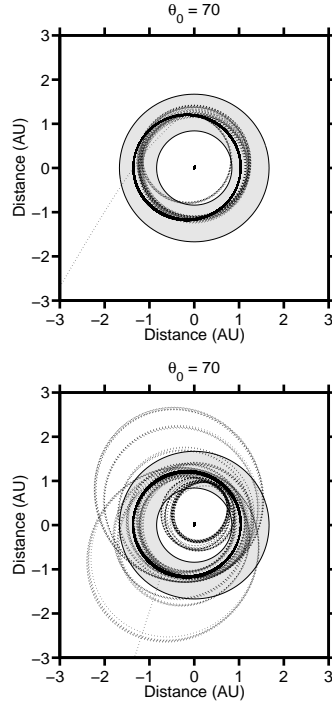


Figure 2.2. Case studies of orbits for a terrestrial planet (dotted line) in HZ (gray area) of HD 188015 based on a simulation time of 1000 years. Note that in both models, the giant planet (solid line) is initially placed at perigee. The starting mass of the terrestrial planets are given as $\delta = 0.5$ at initial mass and increased mass, respectively.

stability of the system. For the particular case shown in Fig. 2.2 it can be seen that increasing the mass alters the orbit of the Earth-mass planet greatly.

2.3 Test of Accuracy of the Code

The orbital stability analysis of both star systems were preformed by running an extensive set of simulations. In each case we allowed the simulation to run for 10^3 yrs due to the ejection of the Earth-mass planet from the system, where a step size of 10^{-4} yr was found to be sufficient for our integration scheme. We arrived at this value by performing detailed test simulations while comparing the ejection times for the Earth-mass planet. These test simulations were carried out by keeping the

Table 2.1. Tests of computer code for HD 20782

Run	τ	T_{sim}	T_{EJ}
(a)	$1 \cdot 10^{-2}$	100	remained within
(b)	$1 \cdot 10^{-3}$	100	85.289
(c)	$1 \cdot 10^{-4}$	100	80.6690
(d)	$1 \cdot 10^{-5}$	100	80.66908
(e)	$1 \cdot 10^{-6}$	100	80.66908

Table 2.2. Tests of computer code of HD 188015

Run	τ	T_{sim}	T_{EJ}
(a)	$1 \cdot 10^{-2}$	1000	7.03
(b)	$1 \cdot 10^{-3}$	1000	7.034
(c)	$1 \cdot 10^{-4}$	1000	7.0347
(d)	$1 \cdot 10^{-5}$	1000	7.03472
(e)	$1 \cdot 10^{-6}$	1000	7.03472

initial conditions the same but varying the step size. It was found that the orbit did not change between the 10^{-4} yr and 10^{-5} yr cases. The following figures and tables demonstrates this comparison.

As can be seen from these figures the orbits of the planets does not change from 10^{-4} to 10^{-5} yr timestep. This means that the 10^{-4} yr timestep is sufficient for all data runs. It can also be seen from Tables 2.1 and 2.2 that the change in ejection time between the 10^{-4} and 10^{-5} yr timesteps are so minor that it is sufficient to use the 10^{-4} yr timestep. It is also noted that the ejection time results between the 10^{-5} and 10^{-6} yr timesteps are almost always identical. The although the 10^{-4} and 10^{-5} yr timesteps are not identical they are the same out to 4 decimal points. Due to the increased amount of time needed between the two sets of timesteps, it was more

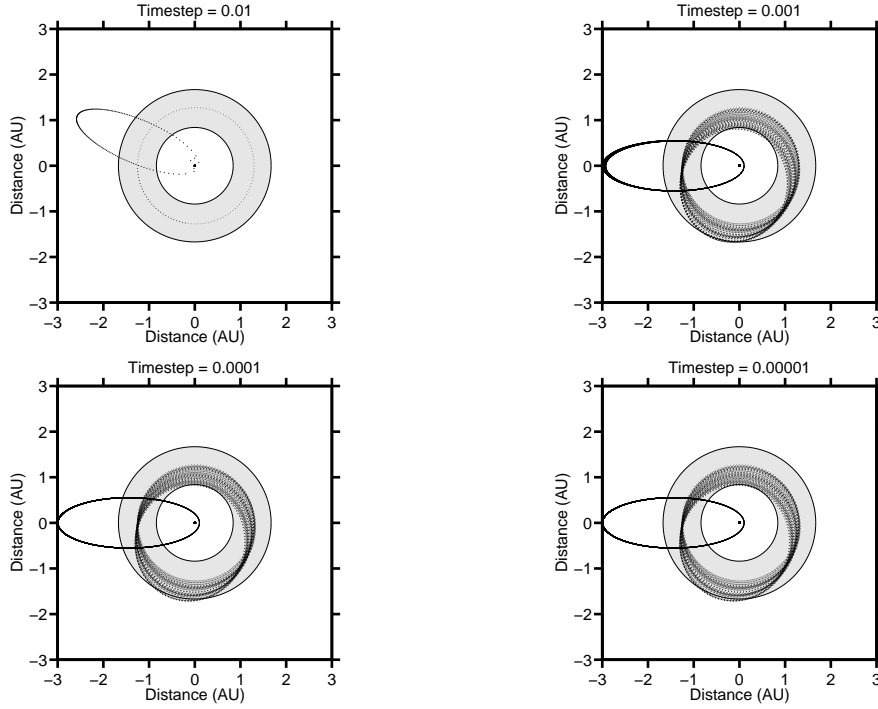


Figure 2.3. Examples of the method used to determine the timestep needed for a precise result for the system HD 20782. Note that the giant planet was initially placed at perigee. The starting position of the Earth-mass planet is given as $\delta = 0.5$ at an angle of 180° .

time effective to use the larger timestep to be able to collect a larger range of data. Therefore the 10^{-4} yr timestep was chosen for all data runs.

It should also be noted that due to the large eccentricity of the star-planet system HD 20782, an adapted timestep should be used for a more precise result. The reason for this is that if we consider an initial aphelion distance of 1 AU and an initial aphelion velocity of $\pi/2$ AU/yr using a time step as small as $\tau = 0.0005$ yr, the total energy varies by over 7% per orbit (Garcia 2000). While this does not seem to affect our results it should be noted that it would increase the efficiency of the program. Due to the physics involved, one only needs a small timestep when the planet is at its closest approach. This would suggest that an adaptive Runge-Kutta Function should

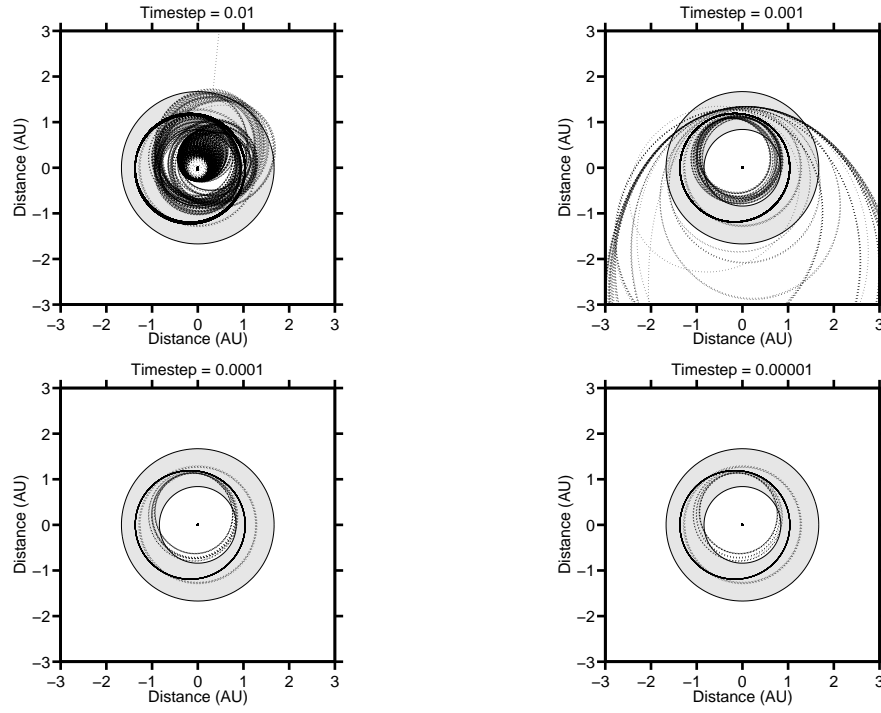


Figure 2.4. Examples of the method used to determine the timestep needed for a precise result for the system HD 188015. Note that the giant planet was initially placed at perigee. The starting position of the Earth-mass planet is given as $\delta = 0.5$ at an angle of 180° .

be used to account for this change. For further applications of this research it would be necessary to implement this change.

CHAPTER 3

RESULTS AND DISCUSSION

In the following two sections we will look at the results obtained from the simulations for each of the two star systems. We will compare various outcomes for the different initial conditions and express our interpretation of the results. In the third section we will then look at the statistics behind the results and draw necessary conclusions from the data obtained.

3.1 Case Study of HD 20782

As previously stated, for each value of $\delta = 0.1$, $\delta = 0.5$, and $\delta = 0.9$, mass of the giant planet, and starting position of the giant planet, 36 simulations were run. In the following figure (Fig. 3.1) we can compare each of these results simultaneously, allowing us to see the variation in results in terms of the log of the ejection time based on the initial conditions. In the first two figures we can see how changing from the perigee to apogee starting position of the giant planet produces extremely different results. In the case of the third plot in Fig. 3.1 we are now comparing the starting positions of the giant planet for the increased mass case. Here the difference in outcomes between starting at apogee or perigee for the giant planet can be compared, noting that the outcomes are radically different, i.e. exhibit chaotic behavior. If we look at this figure in greater detail we can see that in the apogee cases the results appear to be grouped more closely together than in the other two cases. When looking at the perigee and increased mass cases, it can be seen that the results are extremely sporadic. As can be seen from this groupings of plots, it is very difficult to

tell just how the change in starting position of the Earth-mass planet will affect how quickly it is ejected from the HZ.

Several different sets of numerical computations were performed to identify the influence of the starting positions of the giant planet and Earth-mass planet on the outcome of the simulation. In the following, we will showcase various different simulation runs to provide comparisons of the behavior of the Earth-mass planet for various initial conditions. By default, most of these runs are depicted for a simulation time of 10^3 yrs. Figures 3.2 through 3.4 are for the star-planet system HD 20782. In this system, the giant planet is on an extremely elliptical orbit, which typically results in large variations of the gravitational attraction toward the Earth-mass planet. First we will examine two examples for the case $\delta = 0.1$ case and then additional examples for $\delta = 0.5$ and 0.9 . In order to demonstrate how the outcomes vary based on altered initial conditions, we will only change one initial condition between the comparison figures.

The first set that we have chosen to compare is for the apogee and perigee starting positions of the giant planet (Fig. 3.2). As can be seen from the set of plots, this change in starting position by 180° for the giant planet produces a radically different outcome. All of the initial conditions for the Earth-mass planet placed at an angle of 20° remain the same for both figures. When the giant planet is placed at perigee the Earth-mass planet is ejected from the habitable zone after only 23.9 years. If we compare this to the case of the giant planet starting at apogee we see the Earth-mass planet being ejected from the habitable zone in only 7.6 years.

This is interesting due to the fact that in the second case the Earth-mass planet is starting much further away from the giant planet than in the first case, thus being exposed to a significantly smaller amount of gravitational attraction, and yet remains within the habitable zone for a much shorter time than when it starts closer to the giant

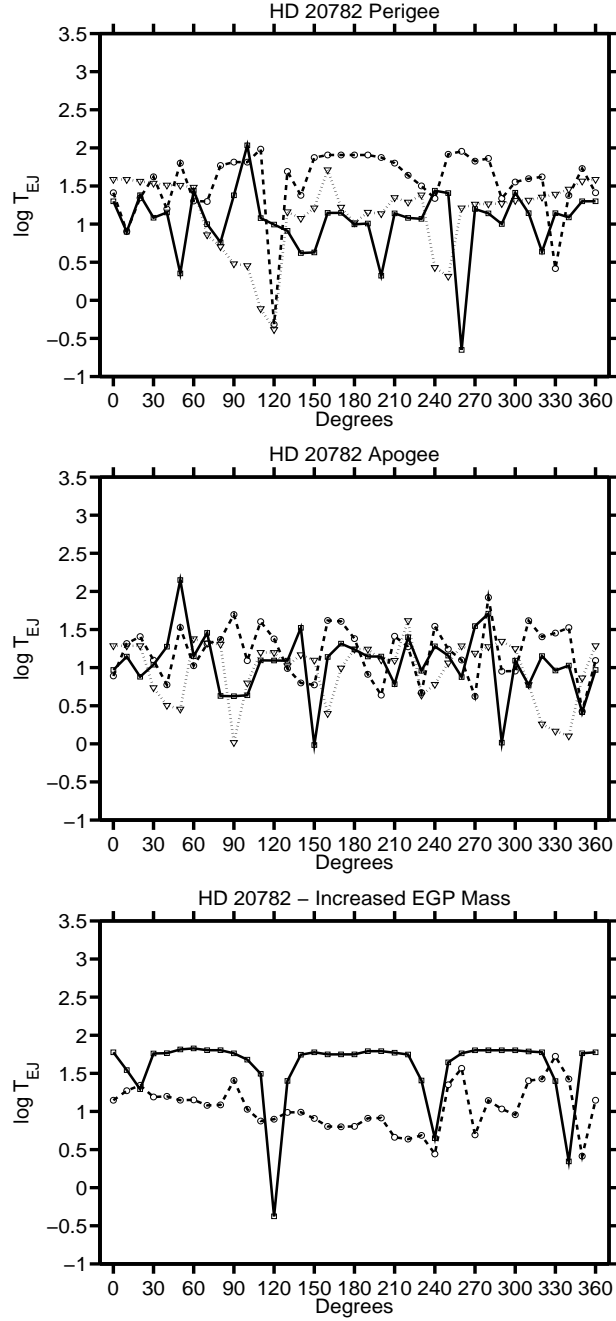


Figure 3.1. Display of $\log T_{EJ}$ for the Earth-mass planet dependent on its starting position, angle θ , for HD 20782. The top figure shows the comparison between the models with starting positions $\delta = 0.1$ (solid line; squares), $\delta = 0.5$ (dashed line; circles), and $\delta = 0.9$ (dotted lines; triangles) with the giant planet originally placed at perigee. The middle figure refers to the same setting, except that the giant planet is now originally placed at apogee. The bottom figure depicts models with the Earth-mass planet at a starting position of $\delta = 0.5$. The mass of the giant planet has now been increased by 30% and is originally placed at perigee (solid line; squares) or at apogee (dashed line; circles).

planet. On the other hand, if the starting angle of the Earth-mass planet is selected as 30° , 40° , and 50° , the encountered ejection times are 12.1 yrs, 14.2 yrs, and 2.3 yrs, respectively, for the giant planet placed at perigee position. However, if the giant planet is originally placed at apogee position, the ejection times of the Earth-mass planets are 10.9 yrs, 141.1 yrs, and 14.1 yrs, respectively. This is a highly intriguing example that small changes in the initial conditions of a non-dissipative system can lead to significantly different outcomes (see also Fig. 3.1).

The next set of comparisons shown deals with the comparison between initial mass and increased mass as well as variation in starting position of the giant planet, as depicted in Fig. 3.3. This figure compares the initial mass and the increased mass for both the perigee and apogee starting positions of the giant planet. In all four cases, the starting position of the Earth-mass planet has been chosen as 10° , a choice which is admittedly highly arbitrary. It can be seen from these plots that changing the starting position from perigee to apogee increases the amount of time the Earth-mass planet is within the habitable zone by almost a factor of three.

However, this is not the case for the increased mass. While the increased mass does increase the amount of time that the Earth-mass planet resides within the habitable zone for the perigee starting position of the giant planet, it reduces the amount of time spent within the habitable zone when the giant planet starts at apogee. It can also be seen from the figure that the changes in starting position and mass of the giant planet produce extremely different outcomes for the orbit of the Earth-mass planet. In three of the four cases it can be seen that the Earth-mass planet is ejected from the habitable zone as well as from the system in a very short amount of time. However, in the case of the giant planet starting at perigee and with an increased mass, it is seen that the Earth-mass planet is ejected from the habitable zone in 34.9 years but still remains to be part of the system. The orbit of the Earth-mass planet

appears to take on a more elliptical path with each close encounter with the giant planet, pushing it farther and farther away from the host star and ultimately the habitable zone.

Figure 3.4 is relatively similar to Fig. 3.2 in respect to what is being compared with the exception of the initial placement of the Earth-mass planet within the habitable zone. For this set of simulations we are now looking at a starting placement of $\delta = 0.9$ and a starting angle of 160° . It can be seen that by changing the starting position of the giant planet, the orbit of the Earth-mass planet is again significantly altered. In the case of apogee the Earth-mass planet is very close to the starting position of the giant planet as can be seen from the early interaction. Due to this interaction, the Earth-mass planet is almost immediately ejected from the system, whereas for the case of perigee it takes a longer period of time before the interaction between the giant planet and the Earth-mass planet causes the Earth-mass planet to be ejected from the system. This was not the case for the case studies depicted in Figs. 3.2 and 3.3. Although the Earth-mass planet started much closer to the perigee starting position of the giant planet, it was seen that when the giant planet started at apogee that the Earth-mass planet was ejected from the habitable zone much more quickly, which is again very surprising. In this case, the difference between the length of stay within the habitable zone is about a factor of 20.

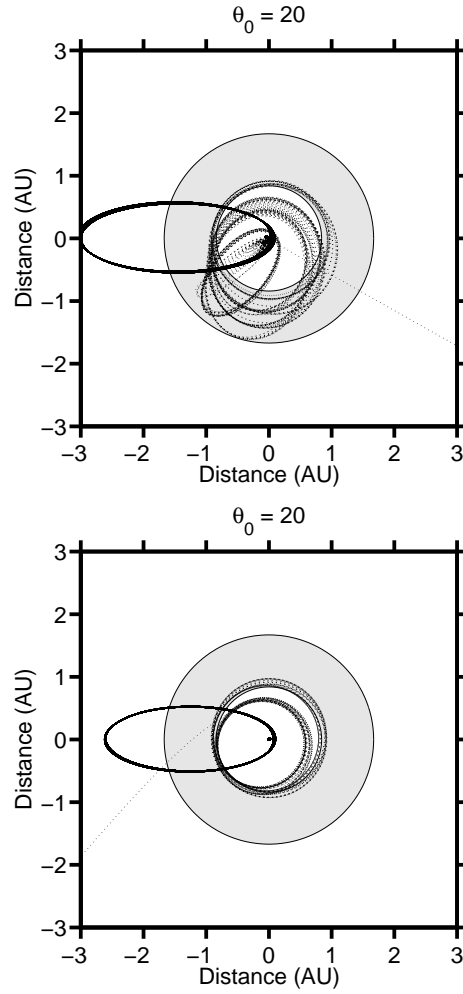


Figure 3.2. Case studies of orbits for an Earth-mass planet (dotted line) in the HZ (gray area) of HD 20782. The starting positions of the Earth-mass planets are given as $\delta = 0.1$ at an angle of 20° . The giant planet (solid line) was initially placed at perigee (top figure) and apogee (bottom figure). The Earth-mass planets were ejected after 23.9 and 7.6 yrs, respectively .

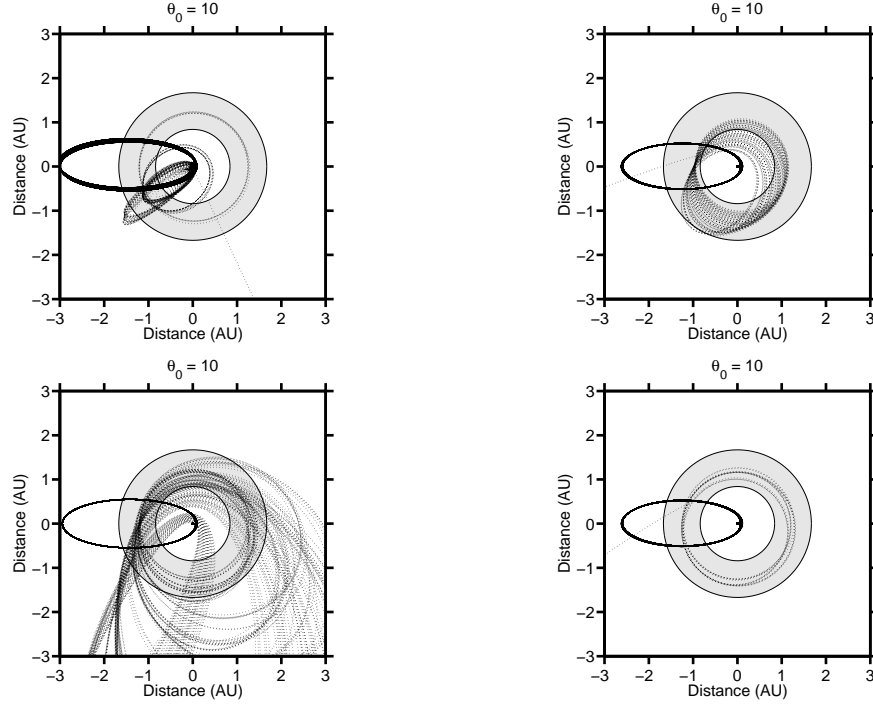


Figure 3.3. Case studies of orbits for an Earth-mass planet (dotted line) in the HZ (gray area) of HD 20782. The starting positions of the Earth-mass planets are given as $\delta = 0.5$ at an angle of 10° . The simulations also refer to different cases for the giant planet (solid line), originally placed at perigee (left column) and apogee (right column) and with minimum mass (top row) and its mass increased by 30% (bottom row), respectively. The Earth-mass planets were ejected after 8.0, 20.7, 34.9, and 18.7 yrs, respectively (from left to right and top to bottom) .

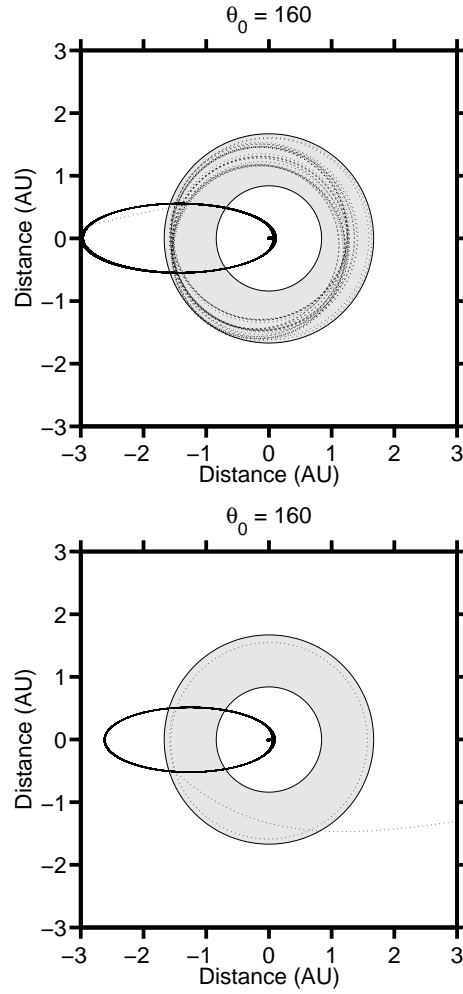


Figure 3.4. Case studies of orbits for an Earth-mass planet (dotted line) in the HZ (gray area) of HD 20782. The starting positions of the Earth-mass planets are given as $\delta = 0.9$ at an angle of 160° . The giant planet (solid line) was initially placed at perigee (top figure) and apogee (bottom figure). The Earth-mass planets were ejected after 51.5 and 2.5 yrs, respectively .

3.2 Case Study of HD 188015

The results obtained from each of the data runs for the star-planet system HD 188015 can be viewed simultaneously in the following figure (Fig. 3.5). This grouping of figures also shows the effects of changing the starting distance of the Earth-mass planet within the habitable zone. It can be seen from this figure that the change between $\delta = 0.1$, $\delta = 0.5$, and $\delta = 0.9$ produces extremely different outcomes in terms of the log of the ejection time. This result can be seen for both the perigee and apogee starting position of the giant planet. In the case of the third plot in (Fig. 3.5) we are now comparing the starting positions of the giant planet for the increased mass case. Here the difference in outcomes between starting at apogee or perigee for the giant planet can be compared, noting that the outcomes are radially different, again implying that the system is exhibiting chaotic behavior.

The next three figures (Figs. 3.6 through 3.8) are the case studies associated with the star system HD 188015 and set up in the same manner as the case studies for HD 20782 in the previous section. In this system, the giant planet has a semimajor axis of $a_p = 1.203$ and a relatively small eccentricity of $e_p = 0.137$ (see Table 1.1), and thus spends all of its time in the stellar habitable zone. Thus, there is typically a stronger gravitational interaction between the giant planet and the Earth-mass planet compared to the system HD 20782, although strong variations in the gravitational force exist owing to the changes in orbital positions of the objects.

We again examine the various starting positions of the Earth-mass planet ranging from $\delta = 0.1, 0.5$ and 0.9 to compare the different outcomes of the simulation runs. The first figure that we examine in greater detail (Fig. 3.6) is somewhat similar to Fig. 3.2 albeit noticeable differences in the star system and initial starting position of the Earth-mass planet. Here we see that for the case of perigee the Earth-mass planet's starting position is far enough away from the position of the giant planet

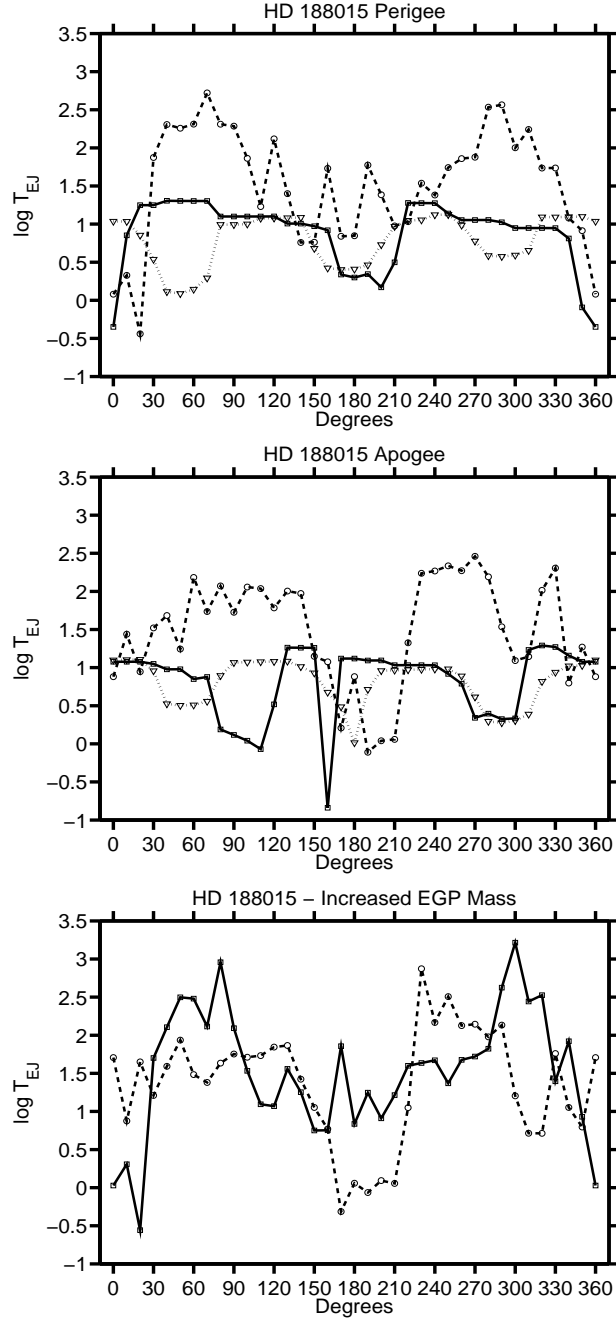


Figure 3.5. Display of $\log T_{EJ}$ for the Earth-mass planet dependent on its starting position, angle θ , for HD 188015. The top figure shows the comparison between the models with starting positions $\delta = 0.1$ (solid line; squares), $\delta = 0.5$ (dashed line; circles), and $\delta = 0.9$ (dotted lines; triangles) with the giant planet originally placed at perigee. The middle figure refers to the same setting, except that the giant planet is now originally placed at apogee. The bottom figure depicts models with the Earth-mass planet at a starting position of $\delta = 0.5$. The mass of the giant planet has now been increased by 30% and is originally placed at perigee (solid line; squares) or at apogee (dashed line; circles).

that it is able to remain within the system. The interactions with the giant planet do however alter the orbit of the Earth-mass planet allowing it to fluctuate between the central part of the habitable zone and being just on the inner border of the habitable zone. This event begins to occur after only 13.8 years. For the case of apogee, we see that the Earth-mass planet and the giant planet start very near to each other causing an interaction to happen almost immediately and ejecting the Earth-mass planet from the system, after only 8.3 years.

Figure 3.7 is again a comparison between the initial mass and the increased mass of the giant planet with the Earth-mass planet originally placed at 160° , and the giant planet placed at either the perigee or the apogee position. For this particular star-planet system we are able to identify a completely different outcome from what we saw with the previous system. The Earth-mass planet spends most of its time within the habitable zone for the perigee starting position of the giant planet with the original mass. However, when the mass is increased, the Earth-mass planet is ejected only after 5.7 years. This means that it is now ejected about 9 times more quickly than in the simulation with the original mass. For the case of apogee, we see that the Earth-mass planet resides within the habitable zone for 11.9 years, but is then ejected more quickly when the mass of the giant planet has been increased. In this case the Earth-mass planet is ejected twice as fast once the mass of the giant planet is increased. It can also be identified from this set of plots that the Earth-mass planet is spending the most time within the habitable zone when it is starting near the perigee starting position, which is also what we found for the first two case studies of the previous star-planet system.

The final set of orbits that we show are for that of a starting case of 40° with an initial starting position of $\delta = 0.9$ within the habitable zone. It can be seen in Fig. 3.8 that the Earth-mass planet is ejected from the system when the initial position of the

giant planet is at perigee, whereas the planet is not necessarily ejected from the system when the giant planet's initial position is at apogee. Nevertheless, in both cases the Earth-mass planets are still almost immediately ejected from the habitable zone. For the starting position of the giant planet at perigee the Earth-mass planet remains within the habitable zone for a length of 1.3 years, while for the case of the giant planet starting at apogee the Earth-mass planet only remains within the habitable zone for 3.3 years. Both of these stays within the habitable zone are extremely short but nonetheless correspond to radically different orbits for the Earth-mass planet.

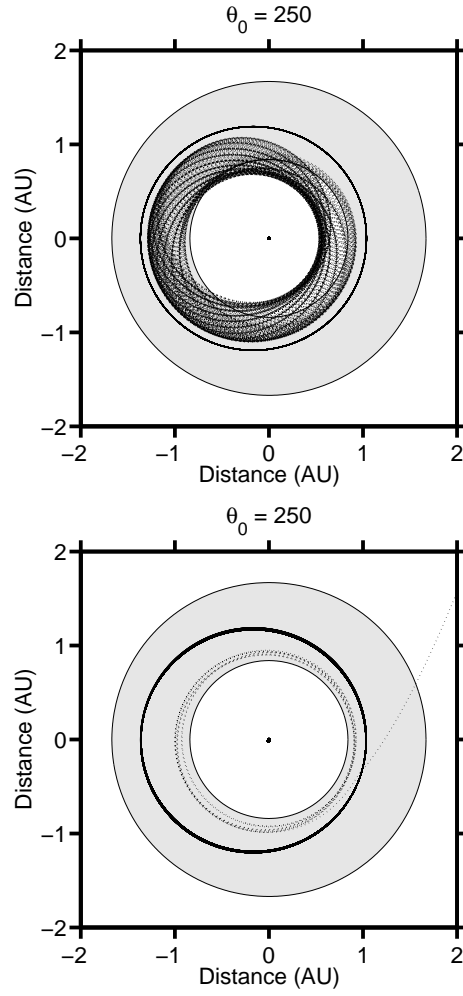


Figure 3.6. Case studies of orbits for an Earth-mass planet (dotted line) in the HZ (gray area) of HD 188015. The starting positions of the Earth-mass planets are given as $\delta = 0.1$ at an angle of 250° . The giant planet (solid line) was initially placed at perigee (top figure) and apogee (bottom figure). The Earth-mass planets were ejected after 13.8 and 8.3 yrs, respectively .

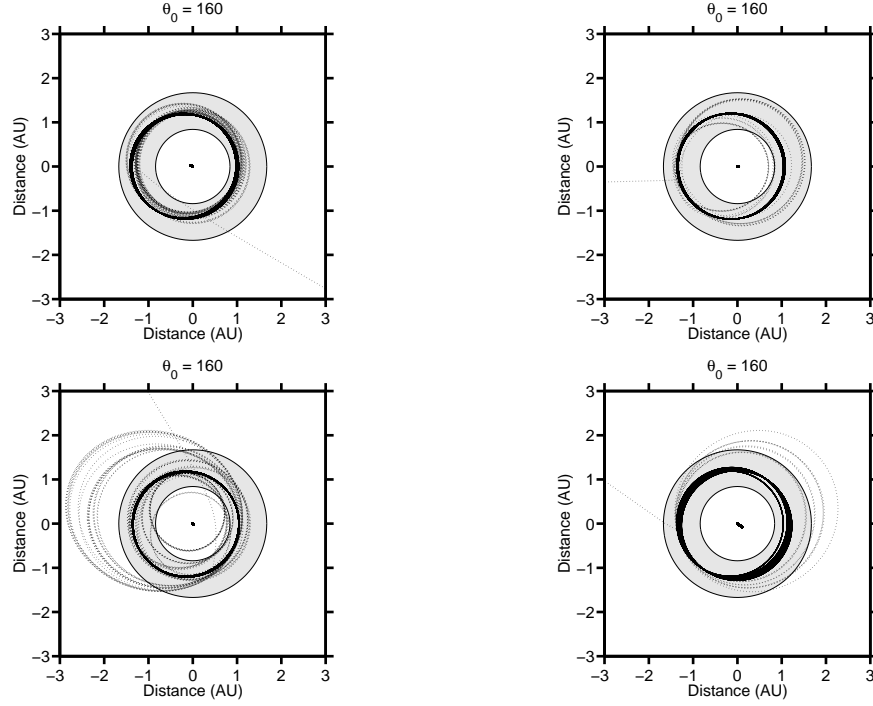


Figure 3.7. Case studies of orbits for an Earth-mass planet (dotted line) in the HZ (gray area) of HD 188015. The starting positions of the Earth-mass planets are given as $\delta = 0.5$ at an angle of 160° . The simulations also refer to different cases for the giant planet (solid line), originally placed at perigee (left column) and apogee (right column) and with minimum mass (top row) and its mass increased by 30% (bottom row), respectively. The Earth-mass planets were ejected after 53.8, 11.9, 5.7, and 5.9 yrs, respectively (from left to right and top to bottom) .

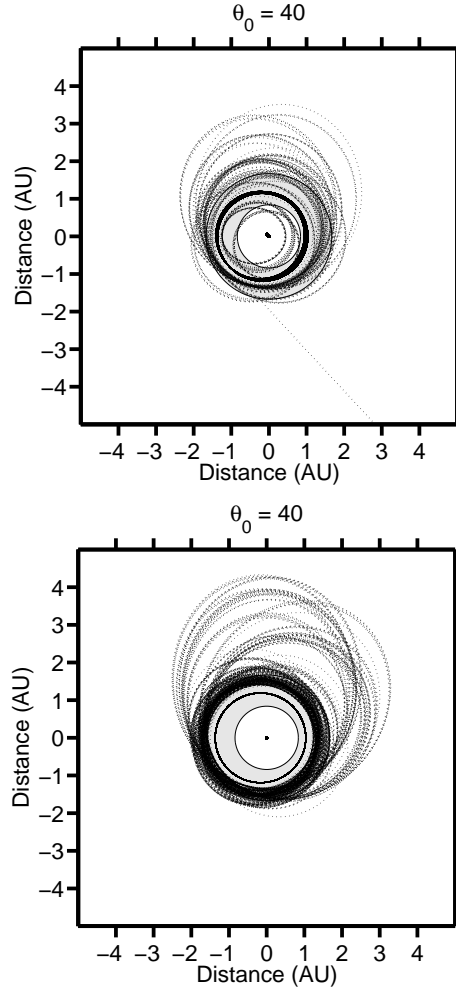


Figure 3.8. Case studies of orbits for an Earth-mass planet (dotted line) in the HZ (gray area) of HD 188015. The starting positions of the Earth-mass planets are given as $\delta = 0.9$ at an angle of 40° . The giant planet (solid line) was initially placed at perigee (top figure) and apogee (bottom figure). The Earth-mass planets were ejected after 1.3 and 3.3 yrs, respectively .

3.3 Statistics of Terrestrial Planet Ejections

In this section we will discuss the statistical significance of the results obtained. The main statistical quantities that we are concerned with are the standard deviation, variance, median, skewness, and kurtosis. We will now discuss the basic meaning of each of these terms, as given from (Freund 1999) chapters 4 and 8, so that we can discuss the results in further detail.

3.3.1 Analysis of Standard Deviation, Median and Variance

The standard deviation of a discrete random variable is the root-mean-square (RMS) deviation of its values from the mean.

If the random variable X takes on N values x_1, \dots, x_N (which are real numbers) with equal probability, then its standard deviation σ can be calculated as follows:

1. Find the mean, \bar{x} , of the values.
2. For each value x_i calculate its deviation $(x_i - \bar{x})$.
3. Calculate the squares of these deviations.
4. Find the mean of the squared deviations. This quantity is the variance σ^2 .

$$\sigma^2 = \frac{1}{N^*} \sum_{i=1}^N (x_i - \bar{x})^2 \quad (3.1)$$

with $N^* = N$ or $N^* = N - 1$ depending on the adopted statistical model.

5. Take the square root of the variance.

This calculation is described by the following formula:

$$\sigma = \sqrt{\frac{1}{N^*} \sum_{i=1}^N (x_i - \bar{x})^2}, \quad (3.2)$$

where \bar{x} is the arithmetic mean of the values x_i , defined as:

$$\bar{x} = \frac{x_1 + x_2 + \dots + x_N}{N} = \frac{1}{N} \sum_{i=1}^N x_i. \quad (3.3)$$

The median is described as the number separating the higher half of the sample, or a probability distribution from the lower half. The median of a finite list of numbers can be found by arranging all the observations from lowest value to highest value and picking the middle one. If there is an even number of observations, the median is not unique, so one often takes the mean of the two middle values. At most half the population have values less than the median and at most half have values greater than the median. If both groups contain less than half the population, then some of the population is exactly equal to the median.

3.3.2 Analysis of Skewness and Excess Kurtosis

Skewness is a measure of symmetry, or more precisely, the lack of symmetry. A distribution, or data set, is symmetric if it looks the same to the left and right of the center point.

Kurtosis is a measure of whether the data are peaked or flat relative to a normal distribution. That is, data sets with high kurtosis tend to have a distinct peak near the mean, decline rather rapidly, and have heavy tails. Data sets with low kurtosis tend to have a flat top near the mean rather than a sharp peak. A uniform distribution would be the extreme case.

The skewness is defined as

$$Skew = \frac{\frac{1}{N} \sum_{i=1}^N (x_i - \bar{x})^3}{\left(\frac{1}{N} \sum_{i=1}^N (x_i - \bar{x})^2 \right)^{\frac{3}{2}}} \quad (3.4)$$

The skewness for a normal distribution is zero, and any symmetric data should have a skewness near zero. Negative values for the skewness indicate data that are skewed left and positive values for the skewness indicate data that are skewed right.

By skewed left, we mean that the left tail is long relative to the right tail. Similarly, skewed right means that the right tail is long relative to the left tail.

The excess kurtosis is defined as

$$XKur = \frac{\frac{1}{N} \sum_{i=1}^N (x_i - \bar{x})^4}{\left(\frac{1}{N} \sum_{i=1}^N (x_i - \bar{x})^2 \right)^2} - 3 \quad (3.5)$$

The kurtosis for a standard normal distribution is three. For this reason, we are using the excess kurtosis definition listed above. This definition is used so that the standard normal distribution has a kurtosis of zero. In addition, with this definition a positive kurtosis indicates a “peaked” distribution and a negative kurtosis indicates a “flat” distribution.

The following tables represent the statistical analysis of the data collected for each of the two star systems. The first two tables that follow show how the standard deviation changes as we increase the increments between data collection. The first column dictates the δ position of the Earth-mass planet, then we have the starting position of the giant planet and the $\sin(i)$ value of the giant planet respectively. From there we then state the mean value for the ejection time of the Earth-mass planet along with its standard deviation. For the case of 90° this implies that there are four values used to create this mean value and standard deviation value. In the case of 45° there are eight values and for the cases of 30° , 20° , and 10° there are 12, 18, and 36 data points respectively. It should be noted that as the increments get smaller, the standard deviation values also get smaller. This is due to the larger sample size. Tables 3.1 and 3.2 both demonstrate this result.

If we take a closer look at Table 3.1 it is worth mentioning that for all but one of the cases, when comparing the 90° increment case and the 10° increment case the

Table 3.1. Ejection Times $T_{\text{Ej}}^{\text{mean}}$ for HD 20782. P represents the perigee case and A represents the apogee case. P* and A* represent the increased mass case of $f(m) = 1.3$.

Positions		Increments									
...	...	90°		45°		30°		20°		10°	
...	...	Value	SD	Value	SD	Value	SD	Value	SD	Value	SD
0.1	P	17.4	3.4	13.4	2.6	17.0	2.3	18.6	5.8	15.7	2.9
0.1	A	16.5	7.8	14.4	3.9	12.6	2.6	16.0	2.7	17.5	4.0
0.5	P	59.6	13.6	39.3	10.6	41.5	8.4	44.3	6.6	48.3	4.6
0.5	A	21.4	12.0	31.8	10.6	19.7	4.2	22.4	4.5	21.6	2.8
0.9	P	17.5	8.8	19.9	4.4	18.5	3.8	20.1	3.4	19.6	2.1
0.9	A	13.3	4.8	9.5	2.7	12.4	2.2	14.5	2.4	12.7	1.4
0.5	P*	59.3	1.9	52.6	6.7	47.8	7.1	47.4	5.6	49.0	3.3
0.5	A*	12.7	5.4	14.4	3.7	13.8	4.2	13.8	2.2	13.9	1.8

values are within one standard deviation of each other. While this result is intriguing, it is more appropriate to use the case of 10° increments so that we do not lose the majority of the data. If we then move on to the 45° increment case we see that each of the values lie within one standard deviation of the final case. Again, this is an intriguing result, but it is important to realize that we would lose a lot of data by using the 45° increment case for our entire study.

If we now look at Table 3.2 in the same way as Table 3.1 we find the same intriguing result. In both tables we find that the only case where the 90° increment case is not within one standard deviation of the 10° case is for that of $\delta = 0.5$, perigee with an increased mass. If we then move onto the 45° increment case we again see that all values are within one standard deviation of the 10° increment case.

The next two tables that follow show the mean, median, standard deviation, skew, and excess kurtosis of the data obtained for the 10° increments cases for the

Table 3.2. Ejection Times $T_{\text{Ej}}^{\text{mean}}$ for HD 188015. P represents the perigee case and A represents the apogee case. P* and A* represent the increased mass case of $f(m) = 1.3$.

Positions		Increments									
...	...	90°		45°		30°		20°		10°	
...	...	Value	SD	Value	SD	Value	SD	Value	SD	Value	SD
0.1	P	6.6	3.6	10.6	2.7	10.5	1.9	11.3	1.5	10.9	1.0
0.1	A	7.1	3.6	10.8	2.5	9.2	1.8	8.7	1.4	9.5	1.0
0.5	P	69.1	51.4	74.9	26.4	73.4	21.6	84.6	23.4	94.2	20.2
0.5	A	89.3	77.7	86.3	38.0	84.8	29.2	71.9	16.3	73.7	13.0
0.9	P	7.3	2.2	8.3	1.7	7.5	1.3	7.9	1.0	7.7	0.7
0.9	A	7.3	3.3	6.9	1.7	7.6	1.2	7.6	1.0	7.6	0.6
0.5	P*	46.0	32.7	111.9	39.7	189.8	139.6	204.4	101.7	147.5	52.3
0.5	A*	62.1	33.1	60.3	22.0	49.8	14.9	43.5	10.5	70.2	22.3

star-planet systems HD 20782 and HD 188015 respectively. It should be noted here that the standard deviation listed in Tables 3.3 and 3.4 are different from that of the standard deviations listed in Tables 3.1 and 3.2. The standard deviations listed in Tables 3.3 and 3.4 are for that of an individual ejection time, meaning we are now using $N^* = N - 1$, whereas the standard deviations listed in Tables 3.1 and 3.2 are for the change in the mean value with increased data set size, using $N^* = N$.

When looking at the skewness of the data it is worthwhile to group the skewness into three different groupings. The first grouping being a strong negative skewness, the second group being a mid-skewness, and the final group being a strong positive skewness. For the case of mid-skewness we will define this range as -0.5 to 0.5 . The strong negative skewness will be anything more negative than -0.5 and the strong positive skewness will be anything greater than 0.5 . When looking at the skewness of the data for the star-planet system of HD 20782 it can be seen that the majority

of the data is skewed to the right with the exception of the $\delta = 0.5$ perigee cases for both the original mass and the increased mass. Both of these cases are skewed to the left, although the $\delta = 0.5$ perigee case with the original mass is extremely close to being a normal distribution. Both cases for the $\delta = 0.1$ are highly skewed to the right and represent the most skewed result of the two star systems. Overall for the star-planet system HD 20782 we find that only one case has a value that has a strong negative skewness. We also find that only two cases have values within our mid-skewness range and five cases where there is a strong positive skewness.

The skewness data for HD 188015 shows a similar result as that of HD 20782. In the case of HD 188015 half of the data is skewed to the left and half of the data is skewed to the right. The data that is skewed to the left is very close to a normal distribution with the most negatively skewed set being -0.3 . This means that all of the negatively skewed data for this star-planet system fits into our mid-skewness category. The positively skewed data is much more skewed than the negatively skewed data, with the increased mass cases being the most positively skewed data for this star system, meaning that all of the positively skewed data has a strong positive skewness. This results in four values residing in the mid-skewness range and four values residing in the strong positive skewness right. This implies that between both star-planet systems there is a tendency to be positively skewed resulting in a right tail that is long relative to the left tail. This strong positive skewness suggests that there are a few extreme cases where the Earth-mass planet remains in the habitable zone for a longer time period than would be expected. This would imply that given the right initial conditions, there is a possibility of an Earth-mass planet residing in an unstable system for enough time for the possibility of life to form given the right system set up.

At this point it is also worthwhile to discuss the excess kurtosis. As previously stated before a positive kurtosis indicates a “peaked” distribution and a negative kurtosis indicates a “flat” distribution. If we take another look at tables 3.3 and 3.4 we see that overall the excess kurtosis is very near zero, with the exception of two extreme cases for both star-planet systems. In both of these cases the excess kurtosis is extremely positive, meaning greater than 10. The two extremely positive excess kurtosis cases for HD 20782 are for the $\delta = 0.1$ cases, while for HD 188015 the two extremely positive excess kurtosis cases are the increased mass cases. This means that these data sets are extremely peaked, otherwise the rest data is fairly uniform and behaves well.

If we now compare this work with that of Fatuzzo et al. (2006) and the statistical stability analysis in the binary system we see a very similar result (see Fig. 3.9). It should be noted here, however, that Fatuzzo et al. (2006) uses $\log T_{\text{Ej}}$ instead of the non log case that we are using. This would imply that any skewness that is reported by Fatuzzo et al. (2006) will be even more greatly positively skewed. Based on the results given by Fatuzzo et al. (2006) we see long tail to the right of the data, i.e. a positive skewness. This skewness implies that there are a few cases in the systems studied where the terrestrial planet remains within the otherwise unstable system for a longer period of time than what would be expected. This is the same result that we have obtained for the single star system. The fact that Fatuzzo et al. (2006) reports a very similar result for the binary star case as we have for the single star case is very remarkable. This would imply that given the right initial conditions, i.e. formation conditions, there is a possibility of a stable system occurring in what otherwise appears to be an unstable system.

The final table shown here (Table 3.5) shows the amount of increase between the minimum and maximum ejection times. The factor represents the amount of

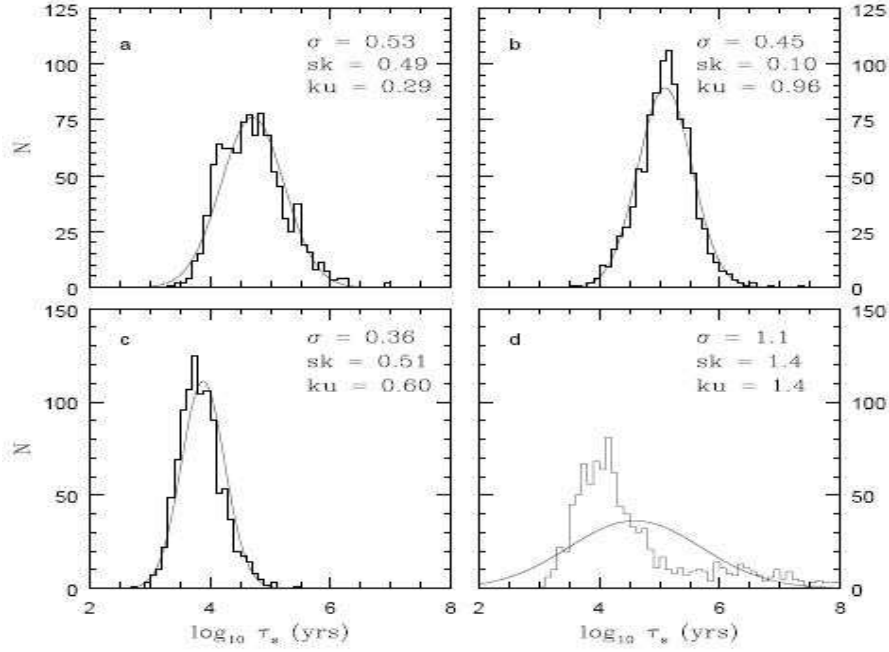


Figure 3.9. Skew and Kurtosis results from Fatuzzo et al.(2006). The solid curve shows a normal distribution with the same mean and width as the computed distributions, normalized to the sample size of $N = 10^3$.

Table 3.3. Statistical Properties of Ejection Times for HD 20782. P represents the perigee case and A represents the apogee case. P* and A* represent the increased mass case of $f(m) = 1.3$.

Positions		Statistical Properties				
...	...	T_{Ej}^{mean}	T_{Ej}^{median}	$SD(T_{Ej})$	$Skew(T_{Ej})$	$XKur(T_{Ej})$
0.1	P	15.7	12.2	17.2	4.3	20.2
0.1	A	17.5	12.4	23.2	4.2	19.5
0.5	P	48.3	46.3	26.9	-0.03	-1.2
0.5	A	21.6	19.6	16.5	1.5	3.1
0.9	P	19.6	18.5	12.5	0.4	-0.4
0.9	A	12.7	12.6	8.4	0.8	1.4
0.5	P*	49.0	57.9	19.0	-1.4	0.6
0.5	A*	13.9	10.7	10.3	1.8	3.8

Table 3.4. Statistical Properties of Ejection Times for HD 188015. P represents the perigee case and A represents the apogee case. P* and A* represent the increased mass case of $f(m) = 1.3$.

Positions		Statistical Properties				
...	...	$T_{\text{Ej}}^{\text{mean}}$	$T_{\text{Ej}}^{\text{median}}$	$\text{SD}(T_{\text{Ej}})$	$\text{Skew}(T_{\text{Ej}})$	$\text{XKur}(T_{\text{Ej}})$
0.1	P	10.9	10.9	6.0	-0.05	-0.9
0.1	A	9.5	10.8	5.8	-0.07	-1.1
0.5	P	94.2	54.4	118.0	1.9	3.5
0.5	A	73.7	41.2	75.8	1.0	0.03
0.9	P	7.7	9.5	4.2	-0.2	-1.6
0.9	A	7.6	8.9	3.7	-0.3	-1.4
0.5	P*	147.5	41.5	305.4	3.6	13.8
0.5	A*	70.2	34.7	129.9	4.0	17.6

change between the actual value of the minimum ejection time and the maximum ejection time. The most extreme case is for that of $\delta = 0.5$ perigee with an increased mass for HD 188015. The factor change is on the order of 6000. Less extreme cases are also noted from this table, where the factor is only on the order of 11. Oddly, we see that the least extreme and most extreme factors are both yielded from the HD 188015 case, which implies chaotic behavior for the entire system. In the case of HD 20782 the factor values range from 20 to 483 while in the case of HD 188015 the factor values range from 11 to 5906 respectively. From this table, no pattern can be seen as to how the starting position affects the amount of change between the minimum and maximum ejection times, so we must therefore conclude that the planet ejection from the system represents chaotic behavior.

Table 3.5. Minimum and Maximum Ejection Times T_{Ej} for HD 20782 and HD 188015. P represents the perigee case and A represents the apogee case. P* and A* represent the increased mass case of $f(m) = 1.3$.

Positions		HD 20782			HD 188015		
...	...	T_{Ej}^{\min}	T_{Ej}^{\max}	Factor	T_{Ej}^{\min}	T_{Ej}^{\max}	Factor
0.1	P	0.22	107.89	483	0.45	20.20	45
0.1	A	0.96	141.07	146	0.14	19.48	135
0.5	P	0.48	96.19	200	0.36	525.35	1446
0.5	A	2.65	83.29	31	0.77	288.65	373
0.9	P	0.41	51.49	125	1.22	13.30	11
0.9	A	1.04	41.28	40	1.03	12.77	12
0.5	P*	0.42	67.22	160	0.28	1635.96	5906
0.5	A*	2.59	52.91	20	5.88	744.47	1532

CHAPTER 4

FURTHER APPLICATION

4.1 The Hill Radius criterion and its validity

As previously mentioned in earlier chapters, the Hill sphere (Hill Radius) refers to the gravitational sphere of influence of one astronomical body such as Earth in the presence of perturbations from another heavier body (Sun) around which it orbits. In the restricted three body problem containing a heavier mass and a lighter mass, the Hill Radius refers to the region around the lighter mass located at x_2 within which the total gravitational influence on an infinitesimal mass will be directed towards the lighter mass (Pillai et al. 2007). The Hill Radius can be derived by making various assumptions and transferring the origin of the coordinate system to the second mass. The following is a derivation for the simplified Hill Radius equation as given by chapter three of Murray & Dermott (2008).

It is first necessary to start with the equations of motion for the three body problem in the synodic system. These equations are given as follows:

$$\ddot{x} - 2n\dot{y} - n^2x = - \left(\mu_1 \frac{x + \mu_2}{r_1^3} + \mu_2 \frac{x - \mu_1}{r_2^3} \right) \quad (4.1)$$

$$\ddot{y} - 2n\dot{x} - n^2y = - \left(\frac{\mu_1}{r_1^3} + \frac{\mu_2}{r_2^3} \right) y \quad (4.2)$$

where

$$\mu_1 = 1 - \frac{m_2}{m_1 + m_2} \quad (4.3)$$

and

$$\mu_2 = \frac{m_2}{m_1 + m_2}. \quad (4.4)$$

with $m_1 > m_2$. For small mass ratios $\mu_1 \approx 1$ and the planar equations of motion become

$$\ddot{x} - 2n\dot{y} - n^2x = -\frac{x}{r_1^3} - \mu_2 \frac{x-1}{r_2^3} \quad (4.5)$$

$$\ddot{y} - 2n\dot{x} - n^2y = -\frac{y}{r_1^3} - \mu_2 \frac{y}{r_2^3} \quad (4.6)$$

Here we define r_1 as the distance from μ_1 to a particle at point P , and r_2 as the distance from μ_2 to the same point P .

We now transform the x axis such that $x \rightarrow 1+x$ leaving the y axis unchanged, and let $\Delta = r_2$. Since we are now considering motion close to the planet we can assume that x , y , and Δ are small quantities of $O(\mu_2^{\frac{1}{3}})$ and $n = 1$. Neglecting higher powers of μ_2 we have $r_1 \approx (1+2x)^{\frac{1}{2}}$. This allows the planar equations of motion to be written as

$$\ddot{x} - 2\dot{y} = \left(3 - \frac{\mu_2}{\Delta^3}\right)x \quad (4.7)$$

$$\ddot{y} + 2\dot{x} = -\frac{\mu_2}{\Delta^3}y \quad (4.8)$$

Equations 4.7 and 4.8 are called *Hill's equations* and were first derived in connection with Hill's work on lunar theory.

Inspection of Eq. (4.7) reveals that the radial force vanishes when $3\Delta^3 = \mu_2$, expressing the equilibrium between the tidal force and the mutual attraction. This leads to the definition of the *Hill's sphere* as the sphere of radius

$$\Delta_H = \left(\frac{\mu_2}{3}\right)^{\frac{1}{3}} \quad (4.9)$$

surrounding the secondary mass.

With this derivation several approximations were taken into account. The form of the Hill Radius used for this thesis is defined as $R_H = a_p(1 - e_p)\sqrt[3]{m_p/3M_\star}$, where

m_p and M_\star are the masses of the giant planet and the central star, respectively, a_p is the semi-major axis of the giant planet and e_p denotes its orbital eccentricity. In this study we are considering the effects of the Hill Radius on the orbital stability of the Earth-mass planet. This study has been considered by Jones et al. (2005) among others but not in the detail that our study is considering.

Please note that other studies of the Hill Radius criterion such as Menou & Tabachnik (2003) and Jones & Sleep (2002) have defined R_H without the $1 - e_p$ term, whereas, von Bloh et al. (2007) consider a more intricate expression in terms of e_p to identify the stability domain in the HZ in the presence of a giant planet on a non-circular orbit. This expression being

$$R_{\text{int}} = a(1 - e) - n_{\text{int}}(e)R_H \quad (4.10)$$

$$R_{\text{ext}} = a(1 + e) + n_{\text{ext}}(e)R_H \quad (4.11)$$

where e is the eccentricity of the giant planet, R_H is defined without the $1 - e_p$ term, and the values of the functions $n_{\text{int}}(e)$ and $n_{\text{ext}}(e)$ are taken from Table 4 in Jones et al. (2005). In this thesis we will not use these alternative expression but we will still investigate the usefulness of the Hill Radius Criterion by checking the behavior of the Earth-mass planet both regarding R_H and $3R_H$.

For our two star-planet systems, HD 20782 and HD 188015, the Hill Radii are calculated to be 8.52×10^{-3} and 7.88×10^{-2} AU, respectively. As part of our study we perform several sets of simulations both for HD 20782 and HD 188015, aimed particularly at exploring the onset of orbital instability for the Earth-mass planet and its ejection from the stellar HZ. As discussed previously, we place the giant planet either at apogee or perigee relative to the host star at the start of each simulation. We then pursue a set of simulations for each system with different initial positions for

the Earth-mass planet insides the stellar HZ also noting that its velocity components are set up to orbit the star on a circular orbit. The distances for the Earth-mass planet from the host star are chosen according to $r_j = r_{\text{HZ},i} + \delta_j \cdot (r_{\text{HZ},o} - r_{\text{HZ},i})$ with $r_{\text{HZ},i}$ as inner radius of the HZ, $r_{\text{HZ},o}$ as outer radius of the HZ and $\delta_j = 0.1, 0.5$, and 0.9 ($j = 1, 2, 3$) as distance parameter. The inner and outer regions of HZ being used are the same as those defined for our own solar system. The reasons for this practice have been discussed in chapter 1. We also produced another set of simulations where the masses of the giant planets for HD 20782 and HD 188015, with a minimum mass of 1.78 and $1.50 M_J$ (Butler et al. 2006), respectively, were increased by a factor of 1.3 . This also leads to an increase of the two Hill Radii by a factor of $\sqrt{1.3}$, i.e., by 14% .

Figures 4.1 and 4.2 display a set of histograms about the ejection of the Earth-mass planet from the HZs of HD 20782 and HD 188015. The models assume starting positions for the giant planet either at its perigee or apogee. Moreover, we check both the R_H and the $3R_H$ criterion concerning the ejection. The starting positions of the Earth-mass planet were always in the middle of the HZ ($\delta = 0.5$), and were forwarded in 10° increments, resulting in 36 models per histogram display. The histograms show different distributions concerning the number of models (out of a total of 36 models) for a given number of in-and-out events for both the R_H and $3R_H$ ejection criterion. As an intriguing result, there is no exclusive spike at event number 1, which would be the correct outcome if the Hill Radius Criterion was applicable. Oddly, as a strange exception, this type of outcome is found for the $3R_H$ case of HD 188015; however, this finding does not affect the main conclusion of this thesis due to the fact that the Earth-mass planet appears to continuously enter and exit the R_H during the time that it is inside the $3R_H$ and is not immediately ejected from the HZ. The histograms show no clear patterns, except that for HD 20782 the majority of models is consistent

with 0 to 3 in-and-out events in regard to the R_H criterion. On the other hand, there is a large number of model simulations, especially for HD 20782, where the Earth-mass planet never enters the one Hill radius domain, but is still ejected from the HZ (Cuntz & Yeager 2009).

Table 4.1 offers another look at our results. Here we calculated the mean and median of the number of in-and-out events concerning R_H prior to the ejection of the Earth-mass planet from the HZ. The findings in this table are consistent with those shown in (figs. 4.1 and 4.2), and show that the Hill Radius Criterion is invalid. This result is obtained regardless if the Earth-mass planet is started in the middle ($\delta = 0.5$) or near the inner ($\delta = 0.1$) or outer ($\delta = 0.9$) edge of the HZ, or if for the mass of the giant planet the minimum mass ($f(m_p) = 1$) or increased mass ($f(m_p) = 1.3$) is used for our models.

Nevertheless, Table 4.1 reveals some surprising behavior. For instance, it is found that for case studies of HD 188015 with $\delta = 0.5$, N_{median} exhibits extraordinary high values, i.e., between about 12 and 35, whereas the values of N_{mean} are quite decent, i.e., between 4.5 and 7.5. This result is due to a few extreme outliers, which strongly affect N_{mean} , but barely N_{median} . For instance, for a case study with $\delta = 0.5$, the giant planet originally at perigee, and $f(m_p) = 1$, it is found that the Earth-mass planet enters and leaves the one Hill Radius domain a total of 111 times prior to its final ejection from the HZ. However, it is also found that it stays within the $3R_H$ domain most of the time. Even more extreme behaviors are found for case studies of $f(m_p) = 1.3$.

It is also worth mentioning that for HD 188015, at first sight, the Hill Radius Criterion seems to work, because for several sets of simulations, we find $N_{\text{median}} = 1$, as predicted (see Table 4.1). However, this interpretation is misleading because the median value has been calculated for the full set of 36 models, obtained by forwarding

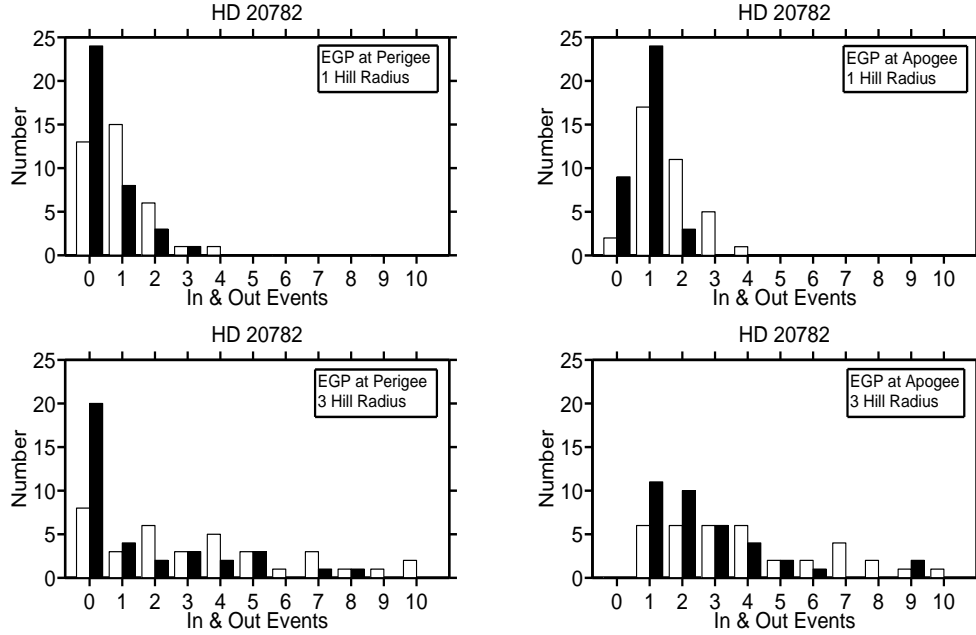


Figure 4.1. Histograms for the ejection of the terrestrial planet from the HZ of HD 20782. The models are based on starting positions for the giant planet given by $\delta = 0.5$ were forwarded in 10° increments, resulting in 36 models per histogram display. The white bars correspond to models of minimum mass for the giant planet, whereas the black bars represent models with an increase mass by a factor of 1.3. Also not that for some histograms there is a small number of outliers beyond event number 10.

the planet in 10° increments, with the other specifications kept constant. Though, if individual models are inspected, there is usually a relative large number of models where the Earth-mass planet never enters the Hill Radius, but is still ejected from the stellar HZ. This type of behavior is offset by various other models where the Earth-mass planet enters and leaves the Hill Radius several times prior to its ejection. Thus, again, we find that the Hill Radius Criterion is an insufficient method for predicting the instability of an Earth-mass planet near a giant planet.

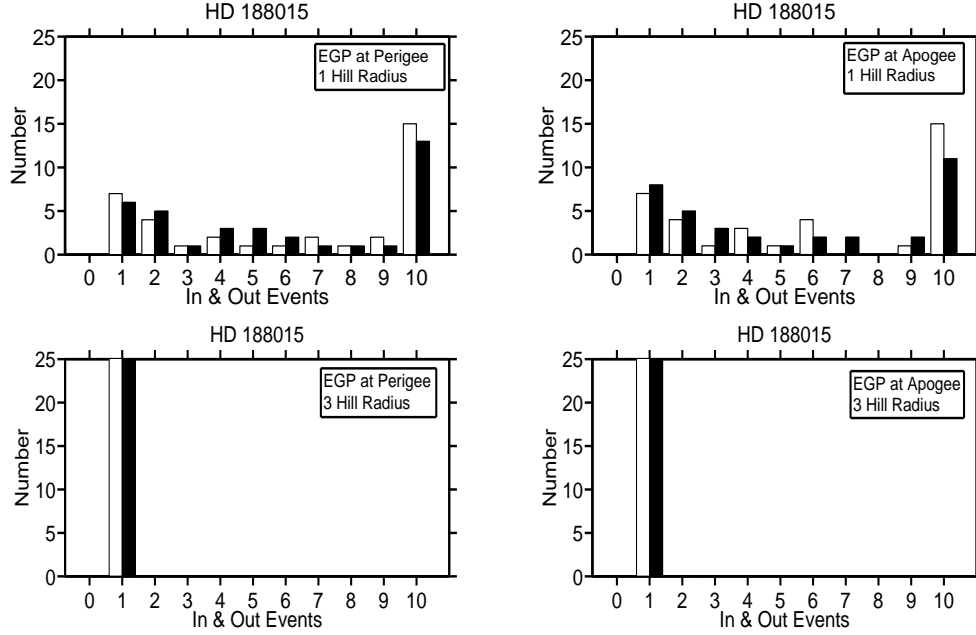


Figure 4.2. Histograms for the ejection of the terrestrial planet from the HZ of HD 188015. The models are based on starting positions for the giant planet given by $\delta = 0.5$ were forwarded in 10° increments, resulting in 36 models per histogram display. The white bars correspond to models of minimum mass for the giant planet, whereas the black bars represent models with an increase mass by a factor of 1.3. Also not that for some histograms there is a small number of outliers beyond event number 10.

Table 4.1. Statistics of R_H Ejections

Positions			HD 20782		HD 188015	
δ	EGP	$f(m_p)$	N_{mean}	N_{median}	N_{mean}	N_{median}
0.1	Perigee	1.0	1.11	1.0	4.72	4.5
0.1	Apogee	1.0	0.94	1.0	4.11	4.0
0.5	Perigee	1.0	0.94	1.0	18.33	7.5
0.5	Apogee	1.0	1.61	1.0	11.58	6.0
0.9	Perigee	1.0	0.36	0.0	2.19	2.0
0.9	Apogee	1.0	0.44	0.0	2.28	3.0
0.5	Perigee	1.3	0.47	0.0	34.89	5.5
0.5	Apogee	1.3	0.83	1.0	14.56	4.5

CHAPTER 5

CONCLUSIONS

The chief goal of our study was to provide a detailed statistical analysis of the ejection of Earth-mass planets from the habitable zones of the solar twins HD 20782 and HD 188015, and to point out various underlying properties. The systems of HD 20782 and HD 188015 possess a giant planet each that crosses into the stellar habitable zone, thus disallowing the existence of habitable terrestrial planets due to the initiation of orbital instabilities; see Noble et al. (2002) for previous results for the system HD 210277, indicating a similar type of behavior. Note that in case of HD 188015, the orbit of the giant planet is essentially circular, whereas in case of HD 20782, it is extremely elliptical. As starting positions for the giant planets, we considered both the apogee and perigee position, whereas the starting positions of the Earth-mass planets were widely varied.

We identified the following statistical properties pertinent to the ejection of the Earth-mass planets from the stellar habitable zones:

1. As a general result it was found that the ejection times are largest if the starting position for the terrestrial planet is placed at $\delta = 0.5$, instead of $\delta = 0.1$ or $\delta = 0.9$, as expected. After comparing the various models, it was found that there were typically no significant differences between the perigee and apogee starting positions for the EGP when the terrestrial planet started at $\delta = 0.1$ or $\delta = 0.9$, but noticeable differences were found for the initial starting positions of $\delta = 0.5$.

2. Concerning the $\delta = 0.5$ case, which is the most interesting case, the ejection times (as gauged by $T_{\text{Ej}}^{\text{mean}}$) are generally longer for HD 188015, which is the quasi-circular case, than for HD 20782, which is the highly elliptical case. The most likely reason is that in this star-planet system, the elliptical orbit of the EGP leads to a larger number of relative close approaches with the terrestrial planet, resulting in its ejection from the HZ.
3. For the star system HD 20782 the mean ejection times seem to be typically between 10 and 20 years with two exceptions both close to 50 years, but the star system HD 188015 has a much wider spread of the mean ejection times ranging from 7.6 years to 147.5 years.
4. We also found that the ejection times for the Earth-mass planets from the habitable zones of HD 20782 and HD 188015, originally placed at the center of the habitable zones, vary by a factor of ~ 200 and ~ 1500 , respectively, depending on the starting positions of the giant and terrestrial planets. If the mass of the giant planet is increased by 30%, the variation in ejection time for HD 188015 increases to a factor of ~ 6000 .
5. Based on the amount of variation in the factor of the ejection times from the habitable zones we have determined that the nature of the behavior is chaotic. Both systems are very sensitive to the initial conditions, in which the planet ejection from the system represents its chaotic behavior.
6. The range of the median ejection time values seem to agree fairly well between the two star systems. The star system HD 20782 has a median range value of 12.2 years to 57.9 years while the star system HD 188015 has a median range value of 8.9 year to 54.4 years.
7. Analysis of skewness of T_{Ej} for the eight models of both stars resulted in showing a significant positive skewness in a large majority of the models. This means

that concerning both stars there are a considerable number of models with relatively long ejection times for the terrestrial planet. This result is of significant astrobiological interest, especially if it can be scaled to other systems. According to this result, there is a possibility of a relatively stable orbit in the parameter of space if the initial conditions allow it. This result is also found in the work of Fatuzzo et al. (2006), although they discuss the skewness of $\log T_{\text{Ej}}$ instead.

8. It was found from the two star systems that there is an overall flat distribution due to the majority of the values having a negative kurtosis. It is worth mentioning, however, that for each star system there are two extreme cases of very positive or “peaked” distributions. In the case of HD 188015 these two cases are for the increased mass cases, while for HD 20782 this result is found for the $\delta = 0.1$ cases.

From our further application investigation of the Hill Radius we were able to determine that the Hill Radius is not a valid criterion in the prediction of orbital stability. Our investigation shows that an Earth-mass planet placed in the HZ of any of the two star-planet systems is eventually ejected; however, the Hill Radius Criterion is of no help for predicting when the ejection takes place. If we take a closer look at studies where the Earth-mass planet was initially placed in the middle of the HZ, i.e., $\delta = 0.5$, we see that in the case of HD 20782 with $f(m_p) = 1$, the Earth-mass planet was ejected from the system in 21% of the cases studied without ever having entered the Hill Radius and in 44% of the cases having entered the Hill Radius once. For $f(m_p) = 1.3$, these numbers amount to 46% and 44%, respectively. In case of HD 188015, the Earth-mass planet entered the Hill radius at least once prior to its ejection from the star-planet system, regardless if the mass of the giant planet was chosen as minimum mass or it was increased by 30%. However, in 79% of the cases

the Earth-mass planet entered the Hill Radius at least twice, again regardless of the mass of the giant planet. In fact, in some of our models for HD 188015, the Earth-mass planet entered the Hill radius of the giant planet more than one hundred times prior to its ejection from the stellar HZ.

A complete analysis comprised of simulations with starting distances of $\delta = 0.1$, 0.5, and 0.9 for the Earth-mass planet and the giant planet either originally at perigee or apogee and assumed to have minimum mass, amounting to a total of 216 models per star, shows the following picture: In case of HD 20782, the Earth-mass planet was ejected from the system in 40% of the cases studied without ever having entered the Hill Radius and in 40% and 20% of the cases when it entered the Hill Radius once or more than once, respectively. In case of HD 188015, these numbers read 0%, 26%, and 74%, respectively. If the mass of the giant planet is raised by 30%, a smaller number of Hill Radius entries is typically required for the Earth-mass planet to be ejected, especially for the system HD 20782.

Thus, the ultimate conclusion of our study entails the highly inconvenient result that future models targeting astrobiological, climatological or geological properties of Earth-mass planets in extra-solar planetary systems need to be based on a self-consistent treatment of planetary orbital stability, rather than a simplistic analytical approximation, to render reliable results.

Overall, we have determined through statistical analysis and analysis of the Hill Radius Criterion that even though a star-planet system appears to be unstable, given the right initial (formation) conditions, it may still be possible for a planet to reside within a HZ for long enough for primitive life to form. Even though the planets were always ejected from the HZ for the two star-planet systems that we studied in great detail, it is encouraging to see a distinct tail in the data, allowing for a few cases to remain within the HZ for a longer period of time. Extrapolating these results to

other star-planet systems may give us a better idea where to look for the most likely candidates of habitable planets.

APPENDIX A
THE CODE

The following is verbatim the code used to calculate the results. It was written by William Jason Eberle and then edited to include information regarding the Hill Radius criterion as was discussed in detail in this thesis. The code follows closely with the program outlined in chapter 3 of Garcia (2000).

A.1 Main Body of Code

```
#include <cstdlib>
#include <math.h>
#include <dirent.h>

//functions for opening, reading, rewinding and closing a directory
#include <dir.h> //creating, deleting, and changing a directory
#include <sstream> //for conversion to string #include <string>
#include "CBody.h"
#include "energy.cpp"
#include "gravrk.cpp"
#include "rk4.cpp"

using namespace std;

double lbound = 0.0;
double ubound = 0.0;

int t_p = 1, lflag = 0, uflag = 0, h1count = 0, h3count = 0, h1flag = 0, h3flag = 0 ;
double lcrosstime = 0.0, ucrosstime = 0.0;

const int LINESIZE = 80; const int debug = 1;

string dtos(double num); //double to string converter int
mkdirtree(double type, double dsp, double Period, double timestep,
double massratio, double TotalMass, double rhonot, double dist); int
RunStuff(CBody *plan, const int nBodies, double param[6], double
tau, double nStep, double dsp); void initial_con (double &t_stop,
int&b_num, double &delta_t, CBody* planet); void
ShiftToCM(CBody*plan);

int main(int argc, char *argv[]) { const int nBodies = 3;
//number of bodies const double pi = acos(-1); const double G =
```

```

4*pi*pi; const double adaptErr = 1e-3;    //for rka CBody
plan[nBodies+1];          // the +1 is so I can count more
intuitivly double param [5+1]; double nStep; double d; double
TimePeriod; double DSP;          //Data Sample period
double tau = 0;
//Dimensions in AU (center of mass coordinates)
double mu; double omega;

int body_num = 0;

//get the initial conditions from "data.in"
initial_con (TimePeriod, body_num, tau, plan);

cout << "-----EXOPLANET-----" << endl;
cout << "\nEnter lower (HZ) boundary [AU]: " ;
cin >> lbound ;
cout << "Enter upper (HZ) boundary [AU]: " ;
cin >> ubound ;
cout << endl;
cout << "Enter the order number of the terrestrial planet as defined in [data.in]." << endl;
cout << "The star is [0], first planet [1], ...etc. ";
cin >> t_p ;
cout<<"\n\n";

DSP = 0.0;

cout<<"The DSP (data sample period) sets how often data is
taken.\n"; cout<<"The DSP must be >= the time step which is:
"<<tau<<endl; while(DSP < tau) { cout<<"\nEnter the DSP: ";
cin>>DSP; if(DSP < tau) cout<<"The DSP (data sample period) must be
>= "<<tau<<endl; }

param[1]=plan[1].GetMass();          //Star
param[2]=plan[3-t_p+1].GetMass();    //Giant Planet
param[3]=plan[t_p+1].GetMass();      //Terrestrial Planet

double Massimo = param[1] + param[2];

```

```

mu = param[2]/Massimo;
param[4] = sqrt(pow(plan[t_p+1].GetPos(X),2) + pow(plan[t_p+1].GetPos(X),2));
d = plan[1].GetPos(X) + plan[3-t_p+1].GetPos(X);
param[5] = d;
nStep = TimePeriod/tau;

mkdirtree(param[0], DSP, TimePeriod, tau, mu, Massimo,param[4], d);

cout<<"Time Period: "<<TimePeriod<<endl;
cout<<"Press any key to continue: \n\n";
cin.ignore(1);

cout << "COMPUTING....." << endl;

RunStuff(plan, nBodies, param, tau, nStep, DSP);

//Print to screen.
cout << "\n\nElapsed time: " << TimePeriod << "yrs" << endl;    /* return elapsed orbital time to screen */

cout << "The output data file is [results.txt]" << endl;
cout << "-----COMPLETE-----.\n";
} //Type 4

    cout<<"The Program Completed Succesfully without incident.\n";
    cout<<"Press any key to quit.";
    cin.ignore(1);
    return EXIT_SUCCESS;
}

//////////End of Main//////////

string dtos(double num) {
    stringstream converter;
    converter << num;
    return converter.str();
}

int mkdirtree(double type, double dsp, double Period, double
timestep, double massratio, double totalmass,double rhonot, double

```

```

dist) {

string dirname;

dirname = "Type " + dtos(type); dirname += " [" + dtos(Period) +
"@"; dirname += dtos(timestep) + "]" "; dirname += "DSP{" + dtos(dsp)
+ "}"; mkdir(dirname.c_str()); chdir(dirname.c_str()); //going in
one dir

dirname = "[mu, M] = [" + dtos(massratio); dirname += ", " +
dtos(totalmass) + "]" "; mkdir(dirname.c_str());
chdir(dirname.c_str()); //going in one more dir

dirname = "[rhonot, D] = [" + dtos(rhonot/dist); dirname += ", " +
dtos(dist) + "]" "; mkdir(dirname.c_str()); chdir(dirname.c_str());
//going in one more dir

mkdir("Data");

return 1; }

int RunStuff(CBody* plan, const int nBodies, double param[6], double
tau, double nStep, double dsp) { double r1plot, th1plot,
r2plot, th2plot,
r3plot, th3plot,
r3xplot, r3yplot,
tplot, tauplot,
p3plot, p3xplot, p3yplot;

//Set up the plotting variable files:
//th1plot, r1plot, potential, kinetic
ofstream th1plotOut("Data/th1plot.txt"),
r1plotOut("Data/r1plot.txt"),
th2plotOut("Data/th2plot.txt"), r2plotOut("Data/r2plot.txt"),
th3plotOut("Data/th3plot.txt"), r3plotOut("Data/r3plot.txt"),
r3xplotOut("Data/r3xplot.txt"), r3yplotOut("Data/r3yplot.txt"),
tplotOut("Data/tplot.txt"),
tauplotOut("Data/tauplot.txt"),

```

```

    potentialOut("Data/potential.txt"),
    kineticOut("Data/kinetic.txt"),
    totalOut("Data/total.txt"),
    p3plotOut("Data/p3plot.txt"),
    p3xplotOut("Data/p3xplot.txt"), p3yplotOut("Data/p3yplot.txt"),
    ParameterOut("Data/Parameter.txt");

if(!th1plotOut || !th2plotOut || !th3plotOut || !r1plotOut || !r2plotOut ||
    !r3plotOut || !r3xplotOut || !r3yplotOut || !tplotOut || !tauplotOut ||
    !potentialOut || !kineticOut || !p3plotOut || !p3xplotOut || !p3yplotOut
    || !ParameterOut)
{
    cerr<<"One or more files could not be opened for writing!\n"
        <<"Press any key to quit.";
    cin.ignore(2);
    exit(1);
}

    ofstream fpOut("results.txt");
    //open files or gracefully exit
    if (!fpOut)
    {
        cout << "!!Output file could not be opened!!" << endl;
        cout<<"Press any key to quit.";
        cin.ignore(3);
        exit(1);
    }

// Output to the screen
double t_run = nStep*tau;
fpOut<<"\n-----INITIAL CONDITIONS-----\n";
fpOut<<"Simulation time duration --> "<<t_run<<"\n\n";
for (int i=1; i <= 3; i++)
{
    fpOut<<"Body "<<i<<":\n";
    fpOut<<"\tMass[Solar units]    --> "<<plan[i].GetMass()<<"\n";
    fpOut<<"\tX-axis Position[AU] --> "<<plan[i].GetPos(X)<<"\n";
    fpOut<<"\tY-axis Position[AU] --> "<<plan[i].GetPos(Y)<<"\n";
    fpOut<<"\tZ-axis Position[AU] --> "<<plan[i].GetPos(Z)<<"\n";
    fpOut<<"\tVX [AU/Yr]          --> "<<plan[i].GetVel(X)<<"\n";

```

```

        fpOut<<"\tVY  [AU/Yr]          --> "<<plan[i].GetVel(Y)<<"\n";
        fpOut<<"\tVZ  [AU/Yr]          --> "<<plan[i].GetVel(Z)<<"\n";
        fpOut<<"-----\n\n";
    }

    fpOut.close();          //close the file for now since we are not writing to it
    //////////////////////////////////////

    ParameterOut<<param[1]<<endl;    //First Mass
    ParameterOut<<param[2]<<endl;    //Second Mass
    ParameterOut<<param[4]<<endl;    //R0
    ParameterOut<<param[5]<<endl;    //D
    ParameterOut<<param[0]<<endl;    //Type of initial conditions
    ParameterOut<<param[3]<<endl;    //small mass

    ParameterOut.close();

    //shift coordinates to Center of Mass coordinates for simulation
    ShiftToCM(plan);

    //starting simulation
    cout<<"Ready to start simulation.  Press any key to
    continue."<<endl; cin.ignore(2); cout<<"Starting
    simulation,..."<<endl<<endl; double time = 0; double tdLast = 0;
    //time to take data double tpsLast = 0;    //time to print data to
    screen
    //*****
    for(double iStep=1; iStep<=nStep; iStep++) { double kinetic = 0;
    double potential = 0; double total = 0;

                                //Defined in energy.cpp
    kinetic = Kinetic(plan,3);    //kinetic of body 3
    potential = Potential(nBodies,plan,3); //potential of body 3
    total = Total(nBodies,plan);    //total energy of system

    //Print to screen only once a year
    if(((time - tpsLast) > (1.0 - 0.5*tau)) && ((time - tpsLast) < (1.0
    + 0.5*tau))) {
        double p1k = plan[1].GetMass()*Kinetic(plan,1);
        double p2k = plan[2].GetMass()*Kinetic(plan,1);

```



```

r3yplot = plan[3].GetPos(Y);
//

p3plot = plan[3].GetV();
//

p3xplot = plan[3].GetVel(X);
//

p3yplot = plan[3].GetVel(Y);
//

tplot = time;
//

tauplot = tau;
//

////////////////////////////////////

////////////////////////////////////

////////////////////////////////////Then stores them in data files////////////////////////////////////
////////////////////////////////////

th1plotOut<<th1plot<<endl;
//

r1plotOut<<r1plot<<endl;
//

th2plotOut<<th2plot<<endl;
//

r2plotOut<<r2plot<<endl;
//

th3plotOut<<th3plot<<endl;
//

r3plotOut<<r3plot<<endl;
//

r3xplotOut<<r3xplot<<endl;
//

r3yplotOut<<r3yplot<<endl;
//

tplotOut<<tplot<<endl;
//

tauplotOut<<tauplot<<endl;
//

potentialOut<<potential<<endl;
//

kineticOut<<kinetic<<endl;
//

totalOut<<total<<endl;
//

p3plotOut<<p3plot<<endl;
//

p3xplotOut<<p3xplot<<endl;
//

p3yplotOut<<p3yplot<<endl;
//

////////////////////////////////////

}

```

```

//When newstate is passed it is the same as state
rk4(time, tau, plan, gravrk);      //integrate using same timestep

double semi = plan[3].GetSemimajor();
double ec = plan[3].GetEcc();

double rhill = semi*(1-ec)*pow(param[2]/(3*param[1]),1/3);
double Trhill = 3*rhill;

double Sep2 = 0.0;
double L2 = pow(lbound,2);
double U2 = pow(ubound,2);

for(int i = 0; i < 3; i++)
    Sep2 += pow(plan[t_p+1].GetPos(i)-plan[1].GetPos(i),2);

if (Sep2 < L2)
{
    if ( lflag == 0)
    {
        lflag = 1;
        lcrosstime = time;
    }
}

if (Sep2 > U2)
{
    if ( uflag == 0)
    {
        uflag = 1;
        ucrosstime = time;
    }
}

double Hsep2 = 0.0;

for(int i = 0; i < 3; i++)
    Hsep2 += pow(plan[t_p+1].GetPos(i)-plan[3].GetPos(i),2);

```

```

if ( Hsep2 < pow(Trhill,2))
{
    if ( h3flag == 0 && lflag ==0 && uflag == 0 )
    {
        h3flag = 1;
        h3count += 1;
    }
}
if( Hsep2 > pow(Trhill,2))
{
    if(h3flag == 1)
    {
        h3flag =0;
    }
}

if ( Hsep2 < pow(rhill,2))
{
    if ( h1flag == 0 && lflag ==0 && uflag == 0 )
    {
        h1flag = 1;
        h1count += 1;
    }
}
if( Hsep2 > pow(rhill,2))
{
    if(h1flag == 1)
    {
        h1flag =0;
    }
}

time+=tau;

} // for (iStep=1; iStep<=nStep; iStep++)

fpOut.open("results.txt",ios::app); //open in append mode

```

```

fpOut<<fixed<<setprecision(5);
if(lflag)
fpOut<<"Terrestrial planet crossed lower bound at t = "<< lcrosstime << " years." << endl;
if(uflag)
fpOut<<"Terrestrial planet crossed upper bound at t = "<< ucrosstime << " years." << endl;
if(!lflag && !uflag)
fpOut<< "Planet " << t_p << " stayed within (HZ)." << endl;
fpOut<<"\n\nLower Bound: "<<lbounds<<" AU.\n";
fpOut<<"Upper Bound: "<<ubounds<<" AU.\n\n";
fpOut<<"Number of times crossed into 3 Hill Radius: "<<h3count<<"\n";
fpOut<<"Number of times crossed into 1 Hill Radius: "<<h1count<<"\n";
fpOut<<"Elapsed time: "<<time<<" years.\n";
fpOut<<"-----COMPLETE-----\n";

fpOut.close();

th1plotOut.close(); r1plotOut.close(); th2plotOut.close();
r2plotOut.close(); th3plotOut.close(); r3plotOut.close();
r3xplotOut.close(); r3yplotOut.close(); tplotOut.close();
tauplotOut.close(); potentialOut.close(); kineticOut.close();
totalOut.close(); p3plotOut.close(); p3xplotOut.close();
p3yplotOut.close();
//Kass's stuff
//"." refers to parent dir
chdir(".");          //go back to mu dir chdir(".");          //go
back to Type dir chdir(".");          //go back to main program dir

} //RunStuff

// Get initial conditions
// - reads initial conditions from "data.in"

void initial_con (double &t_stop, int &b_num, double &delta_t,
CBody* planet) {
    ifstream fpIn("data.in");
    char buff[LINESIZE];          // setup file reading buffers

    if (!fpIn)                   // open "data.in" file or exit gracefully

```

```

{
    cout << "Data.in  could not be opened!!" << endl;
    cout<<"Press any key to quit.";
    cin.ignore(2);
    exit(1);
}

//This section reads the time duration, step and number
//of bodies from the dat file.

fpIn.getline( buff, LINESIZE, ':');          // read line from the file
fpIn.getline( buff, LINESIZE);
t_stop = atof (buff);                        // convert to numeric
if ( debug == 1)                             // debug output
    cout << "Time stop: "<<t_stop << endl;    // etc.....

fpIn.getline( buff, LINESIZE, ':');          // read line from the file
fpIn.getline( buff, LINESIZE);
delta_t = atof (buff);
if ( debug == 1)
    cout << "Time step: "<<delta_t << endl;

fpIn.getline( buff, LINESIZE, ':');          // read line from the file
fpIn.getline( buff, LINESIZE);
b_num = atoi (buff);
if ( debug == 1)
    cout << "Number of bodies: "<<b_num << endl<<endl;

/*
* This section reads the planet initial conditions
* from the data file.
*/

for (int counter = 1; counter <= b_num; counter++)
{
    fpIn.getline( buff, LINESIZE);

```

```

fpIn.getline( buff, LINESIZE, ':');          // read line from the file
fpIn.getline( buff, LINESIZE);
planet[counter].SetMass(atof(buff));
if ( debug == 1)
    cout << "Planet "<<counter<<" Mass: "<<planet[counter].GetMass() << endl;

    cout<<"Planet "<<counter<<"Position vector: <";
for(int s = 0; s < 3; s++)
{

fpIn.getline( buff, LINESIZE, ':');          // read line from the file
fpIn.getline( buff, LINESIZE);
planet[counter].SetPos(s,atof(buff));
if ( debug == 1)
    cout << planet[counter].GetPos(s)<<" ";
}
cout<<">"<<endl;

    cout<<"Planet "<<counter<<"Velocity vector: <";
for(int s = 0; s < 3; s++)
{

fpIn.getline( buff, LINESIZE, ':');          // read line from the file
fpIn.getline( buff, LINESIZE);
planet[counter].SetVel(s,atof(buff));
if ( debug == 1)
    cout << planet[counter].GetVel(s)<<" ";
}
cout<<">"<<endl;

if ( debug == 1)
    cout<<"End planet # "<<counter<<":\n\n";
}

fpIn.getline( buff, LINESIZE, ':');          // read line from the file
fpIn.getline( buff, LINESIZE);
planet[3].SetSemimajor(atof(buff));
if ( debug == 1)
{

```

```

        cout<<"Semimajor Axis: ";
        cout << planet[3].GetSemimajor()<<" \n";
    }

    fpIn.getline( buff, LINESIZE, ':');           // read line from the file
    fpIn.getline( buff, LINESIZE);
    planet[3].SetEcc(atoi(buff));
    if ( debug == 1)
    {
        cout<<"Eccentricity: ";
        cout << planet[3].GetEcc()<<" \n";
    }

    fpIn.close();

    if ( debug == 1)
    {
        cout<<"Take a moment to confirm this is correct.\n"
            <<"Press any key to continue: \n";
        cin.ignore(2);
    }
}

// Initial_out
//      - Outputs the initial conditions to the screen

void ShiftToCM(CBody* plan) {
    double TotalMass = 0;
    double CM[3] = {0.0, 0.0, 0.0};
    double VCM[3] = {0.0, 0.0, 0.0};

    for(int i = 1; i <=3; i++)
        TotalMass += plan[i].GetMass();

    for(int p = 0; p <3; p++)
    {
        for(int i = 1; i <=3; i++)
        {

```

```

        CM[p] += plan[i].GetMass()*plan[i].GetPos(p);
        VCM[p] += plan[i].GetMass()*plan[i].GetVel(p);
    }

    CM[p] /= TotalMass;
    VCM[p] /= TotalMass;
}

for(int p = 0; p <3; p++)
{
    for(int i = 1; i <=3; i++)
    {
        plan[i].SetPos(p,plan[i].GetPos(p) - CM[p]);
        plan[i].SetVel(p,plan[i].GetVel(p) - VCM[p]);
    }
}
}

```

A.2 Celestial Body Class [Cbody.h]

This file defines the class CBody which packages all the information about a celestial body such as a star or planet into one data type.

```

//Class for celestial bodys
#ifndef CBODY_H #define CBODY_H

enum State{X, Y, Z};

//X = 0, Y = 1, Z = 2

class CBody {
    private:
        double mass;
        double pos[3];
        double Tpos[3];
        double vel[3];
        double Tvel[3];
        double acc[3];
        double magR;
        double magV;
        double magA;

```

```

    double Radius;
    double semimajor;
    double ecc;

public:
    CBody(void);
    void SetMass(double);
    double GetMass(void);
    int SetPos(double, double, double);
    int SetPos(int, double);
    double GetPos(int);
    void SetTPos(double, double, double);
    int SetTPos(int, double);
    double GetTPos(int);
    double GetR(void);
    void SetVel(double, double, double);
    int SetVel(int, double);
    double GetVel(int);
    void SetTVel(double, double, double);
    int SetTVel(int, double);
    double GetTVel(int);
    double GetV(void);
    void SetAcc(double, double, double);
    int SetAcc(int, double);
    double GetAcc(int);
    double GetA(void);
    void SetSemimajor(double);
    double GetSemimajor(void);
    void SetEcc(double);
    double GetEcc(void);
    void Prepare(void);
    void Update(void);
};

CBody::CBody(void) {
    mass = 0;
    magR = 0;
    magV = 0;
    magA = 0;

```

```

    Radius = 0;

    for(int i = 0; i < 3; i++)
    {
        pos[i] = 0;
        Tpos[i] = 0;
        vel[i] = 0;
        Tvel[i] = 0;
        acc[i] = 0;
    }
}

void CBody::SetMass(double M) {
    mass = M;
}

double CBody::GetMass(void) {
    return mass;
}

int CBody::SetPos(double x, double y, double z) {
    pos[0] = x;
    pos[1] = y;
    pos[2] = z;

    return 1;
}

int CBody::SetPos(int s, double val) {
    if(s >= 0 && s < 3)
    {
        pos[s] = val;
        return 1;
    }
    return 0;
}

double CBody::GetPos(int s) {

```

```

        if(s >= 0 && s < 3)
            return pos[s];
        else
        {
            exit(1);
        }
    }

void CBody::SetTPos(double tx, double ty, double tz) {
    Tpos[0] = tx;
    Tpos[1] = ty;
    Tpos[2] = tz;
}

int CBody::SetTPos(int s, double val) {
    if(s >= 0 && s < 3)
    {
        Tpos[s] = val;
        return 1;
    }
    return 0;
}

double CBody::GetTPos(int s) {
    if(s >= 0 && s < 3)
        return Tpos[s];
    else
    {
        exit(1);
    }
}

double CBody::GetR(void) {
    magR = sqrt(pos[0]*pos[0] + pos[1]*pos[1] + pos[2]*pos[2]);
    return magR;
}

void CBody::SetVel(double vx, double vy, double vz) {
    vel[0] = vx;

```

```

        vel[1] = vy;
        vel[2] = vz;
    }

int CBody::SetVel(int s, double val) {
    if(s >= 0 && s < 3)
    {
        vel[s] = val;
        return 1;
    }
    return 0;
}

double CBody::GetVel(int s) {
    if(s >= 0 && s < 3)
        return vel[s];
    else
    {
        exit(1);
    }
}

void CBody::SetTVel(double tvx, double tvy, double tvz) {
    Tvel[0] = tvx;
    Tvel[1] = tvy;
    Tvel[2] = tvz;
}

int CBody::SetTVel(int s, double val) {
    if(s >= 0 && s < 3)
    {
        Tvel[s] = val;
        return 1;
    }
    return 0;
}

double CBody::GetTVel(int s) {
    if(s >= 0 && s < 3)

```

```

        return Tvel[s];
    else
    {
        exit(1);
    }
}

double CBody::GetV(void) {
    magV = sqrt(vel[0]*vel[0] + vel[1]*vel[1] + vel[2]*vel[2]);
    return magV;
}

void CBody::SetAcc(double ax, double ay, double az) {
    acc[0] = ax;
    acc[1] = ay;
    acc[2] = az;
}

int CBody::SetAcc(int s, double val) {
    if(s >= 0 && s < 3)
    {
        acc[s] = val;
        return 1;
    }
    return 0;
}

double CBody::GetAcc(int s) {
    if(s >= 0 && s < 3)
        return acc[s];
    else
    {
        exit(1);
    }
}

double CBody::GetA(void) {
    magA = sqrt(acc[0]*acc[0] + acc[1]*acc[1] + acc[2]*acc[2]);
    return magA;
}

```

```

}

void CBody::SetSemimajor(double sm) {
    semimajor = sm;
}

double CBody::GetSemimajor(void) {
    return semimajor;
}

void CBody::SetEcc(double e) {
    ecc = e;
}

double CBody::GetEcc(void) {
    return ecc;
}

void CBody::Prepare(void) {
    for(int i=0; i < 3; i++)
    {
        Tpos[i] = pos[i];
        Tvel[i] = vel[i];
    }
}

void CBody::Update(void) {
    for(int i=0; i < 3; i++)
    {
        pos[i] = Tpos[i];
        vel[i] = Tvel[i];
    }
}

#endif

```

A.3 Derivative Function [gravrk.cpp]

```
#include "CBody.h"
```

```

void gravrk(double t, CBody* planet, double deriv[][6]) {
// Returns right-hand side of Kepler ODE; used by Runge-Kutta routines
// Inputs
//   t           Time (not used)
//   planet       State array of CBody objects
// Output
//   deriv        Derivatives [dr(1)/dt dr(2)/dt dv(1)/dt dv(2)/dt]
const double pi = acos(-1); double sepex[3]; //seperation vectors #:
n(n-1)/2 where n = 3 bodies in this case double sepey[3]; //seperated
into x, y and z components double sepez[3]; double SEP[3];
//magnitude of seperation vector enum State{ X, Y, Z};

for(int p = 1; p <= 3; p++) { double accelx = 0; double accely = 0;
double accelz = 0;
//$$$$$$$$$$$$$$$$$$$$ Calculate the Force due to others $$$$$$$$$$$$$$$$$$
    for(int j=1; j<= 3; j++)
    {
        if(j!=p)
        {
            //X, Y, and Z components of seperation vector for force on p due to j
            //at temporary position state
            sepex[j] = planet[j].GetTPos(X)-planet[p].GetTPos(X);    //X
            sepey[j] = planet[j].GetTPos(Y)-planet[p].GetTPos(Y);    //Y
            sepez[j] = planet[j].GetTPos(Z)-planet[p].GetTPos(Z);    //Z

            SEP[j]=sqrt(sepex[j]*sepex[j]+sepey[j]*sepey[j]+sepez[j]*sepez[j]); //magnitude of seperation vector
            /* Compute acceleration
            double GM_R3 = 4*pi*pi*planet[j].GetMass()/(SEP[j]*SEP[j]*SEP[j]);
            accelx += GM_R3*sepex[j];
            accely += GM_R3*sepey[j];
            accelz += GM_R3*sepez[j];
        } //if j not equal to p
    } //for over j

    /* Return derivatives [dx/dt dy/dt dz/dt dvx/dt dvy/dt dvz/dt]
    deriv[p][0] = planet[p].GetTVel(X);
    deriv[p][1] = planet[p].GetTVel(Y);
    deriv[p][2] = planet[p].GetTVel(Z);

```

```

    deriv[p][3] = accelx;
    deriv[p][4] = accely;
    deriv[p][5] = accelz;
} //for over p } //gravrk

```

A.4 Runge-Kutta Integrator (4^{th} order) [rk4.cpp]

```

void rk4(double t, double tau, CBody* planet,
        void (*derivsRK)(double t, CBody* planet, double deriv[][6]))
{
    // Runge-Kutta integrator (4th order)
    // Inputs
    //  t           Independent variable (usually time)
    //  tau         Step size (usually time step)
    //  planet      State array of CBody objects
    //  derivsRK    Right hand side of the ODE; derivsRK is the
    //              name of the function which returns dx/dt
    //              Calling format derivsRK(t,planet,dxdt).
    // Output
    //  planet      New state of planet array after a step of size tau

    int i;
    double F1[3+1][6], F2[3+1][6], F3[3+1][6], F4[3][6];

    for(int p = 1; p<=3; p++)
        planet[p].Prepare();           //sets tempstate equal to state

    /* Evaluate F1 = f(x,t).
    (*derivsRK)(t, planet, F1 ); //integrates tempstate

    /* Evaluate F2 = f( x+tau*F1/2, t+tau/2 ).
    double half_tau = 0.5*tau;
    double t_half = t + half_tau;

    for(int p = 1; p<=3; p++) {
        //increment up tempstate
        planet[p].SetTPos(X, planet[p].GetPos(X) + half_tau*F1[p][0]);
        planet[p].SetTPos(Y, planet[p].GetPos(Y) + half_tau*F1[p][1]);
    }
}

```

```

    planet[p].SetTPos(Z, planet[p].GetPos(Z) + half_tau*F1[p][2]);
    planet[p].SetTVel(X, planet[p].GetVel(X) + half_tau*F1[p][3]);
    planet[p].SetTVel(Y, planet[p].GetVel(Y) + half_tau*F1[p][4]);
    planet[p].SetTVel(Z, planet[p].GetVel(Z) + half_tau*F1[p][5]);
}

```

```

(*derivsRK)(t_half, planet, F2 ); //integrates tempstate

```

```

/* Evaluate F3 = f( x+tau*F2/2, t+tau/2 ).

```

```

for(int p = 1; p<=3; p++) {
    planet[p].Prepare();          //sets tempstate equal to state
    //increment up tempstate
    planet[p].SetTPos(X, planet[p].GetPos(X) + half_tau*F2[p][0]);
    planet[p].SetTPos(Y, planet[p].GetPos(Y) + half_tau*F2[p][1]);
    planet[p].SetTPos(Z, planet[p].GetPos(Z) + half_tau*F2[p][2]);
    planet[p].SetTVel(X, planet[p].GetVel(X) + half_tau*F2[p][3]);
    planet[p].SetTVel(Y, planet[p].GetVel(Y) + half_tau*F2[p][4]);
    planet[p].SetTVel(Z, planet[p].GetVel(Z) + half_tau*F2[p][5]);
}

```

```

(*derivsRK)(t_half, planet, F3 ); //integrates tempstate

```

```

/* Evaluate F4 = f( x+tau*F3, t+tau ).

```

```

    double t_full = t + tau;
    for(int p = 1; p<=3; p++) {
        planet[p].Prepare();          //sets tempstate equal to state
        //increment up tempstate
        planet[p].SetTPos(X, planet[p].GetPos(X) + tau*F3[p][0]);
        planet[p].SetTPos(Y, planet[p].GetPos(Y) + tau*F3[p][1]);
        planet[p].SetTPos(Z, planet[p].GetPos(Z) + tau*F3[p][2]);
        planet[p].SetTVel(X, planet[p].GetVel(X) + tau*F3[p][3]);
        planet[p].SetTVel(Y, planet[p].GetVel(Y) + tau*F3[p][4]);
        planet[p].SetTVel(Z, planet[p].GetVel(Z) + tau*F3[p][5]);
    }

```

```

    (*derivsRK)(t_full, planet, F4 );

```

```

for(int p = 1; p<=3; p++) {
    planet[p].Prepare();          //RE-sets tempstate equal to state
    /* Return x(t+tau) computed from fourth-order R-K.

```

```

//increment up tempstate
planet[p].SetTPos(X, planet[p].GetTPos(X) + tau/6.*(F1[p][0] +
F4[p][0] + 2.*(F2[p][0]+F3[p][0]))); planet[p].SetTPos(Y,
planet[p].GetTPos(Y) + tau/6.*(F1[p][1] + F4[p][1] +
2.*(F2[p][1]+F3[p][1]))); planet[p].SetTPos(Z, planet[p].GetTPos(Z)
+ tau/6.*(F1[p][2] + F4[p][2] + 2.*(F2[p][2]+F3[p][2])));
planet[p].SetTVel(X, planet[p].GetTVel(X) + tau/6.*(F1[p][3] +
F4[p][3] + 2.*(F2[p][3]+F3[p][3]))); planet[p].SetTVel(Y,
planet[p].GetTVel(Y) + tau/6.*(F1[p][4] + F4[p][4] +
2.*(F2[p][4]+F3[p][4]))); planet[p].SetTVel(Z, planet[p].GetTVel(Z)
+ tau/6.*(F1[p][5] + F4[p][5] + 2.*(F2[p][5]+F3[p][5])));
}

for(int p=1; p<=3; p++)
{
planet[p].Update(); //the idea here is change after all steps are made instead
} //of changing while steps are being made,
//which hopefully reduces error propagation
}

```

A.5 Energy Calculator [energy.cpp]

```

double Kinetic(CBody* param, int i); double Potential(int n, CBody*
param, int i); double Total(int n, CBody* param);

// n      the total number of Celestial Bodies
// param  array of CBody data structures
// i      index number of a specific body

// 5/12/2008 I took out the mass parameter so
// these functions acctually return the energy/unit mass
double Kinetic(CBody* param, int i) { double kinetic=0;

    kinetic += 0.5*param[i].GetV()*param[i].GetV();
    return kinetic;
} //Kinetic

double Potential(int n, CBody* param, int i) { const double pi =
acos(-1); double G = 4*pi*pi; double potential=0; double sepex[6];

```

```

//seperation vectors #: n(n-1) where n = 3 bodies in this case
        //(different directions counted)
double sepey[6];    //seperated into x, y and z components double
sepez[6]; double SEP[6]; //magnitude of seperation vector

for(int j = 1; j <= n; j++) { if(i!=j)
    {
        //X, Y and Z components of seperation vector for force on i due to j
        sepex[j] = param[j].GetPos(X)-param[i].GetPos(X); //X
        sepey[j] = param[j].GetPos(Y)-param[i].GetPos(Y); //Y
        sepez[j] = param[j].GetPos(Z)-param[i].GetPos(Z); //Z
        SEP[j]=sqrt(sepex[j]*sepex[j]+sepey[j]*sepey[j] + sepez[j]*sepez[j]); //magnitude of seperation vector
        potential+=-G*param[j].GetMass()/SEP[j]; //adds up total potential of all bodies
    } //if
} //for
    return potential;
} //Potential

double Total(int n, CBody* param) {
    double total=0;
    for(int i=1; i<=n; i++)
        total += Kinetic(param,i) + Potential(n,param,i)/2; //n(n-1)/2 interactions for potential
    return total;
} //Total

```

REFERENCES

- Asghari, N., et al. 2004, A&A, 426, 353
- Baglin, A. 2003, Adv. Space Res., 31, 345
- Borucki, W. J., et al. 2003, in Towards Other Earths: *DARWIN/TPF* and the Search for Extrasolar Terrestrial Planets, ed. M. Fridlund, T. Henning, & H. Lacoste (ESA SP-539; Noordwijk: ESA), 69
- Borucki, W. J., et al. 2007, in ASP Conf. Ser. 366, Transiting Extra-Solar Planets Workshop, ed. C. Afonso, D. Weldrake, & T. Henning (San Francisco: ASP), 309
- Butler, R. P., et al. 2006, ApJ, 646, 505
- Carroll, B. W., & Ostlie, D. A., An Introduction To Modern Astrophysics 2nd ed., San Francisco, California, Pearson/Addison Wesley, Inc 2006
- Catanzarite, J., Shao, M., Tanner, A., Unwin, S., & Yu, J. 2006, PASP, 118, 1319
- Cockell, C.S., *et al.* 2009, Astrobiology, 9, 1
- Cuntz, M., von Bloh, W., Bounama, C., & Franck, S. 2003, Icarus, 162, 214
- Cuntz, M., Eberle, J., & Musielak, Z. E. 2007, ApJ, 669, L105
- Cuntz, M. & Yeager, K.E. 2009, ApJ, 697, L86
- Eberle, J., Cuntz, M., & Musielak, Z. E. 2008, A&A, 489, 1329
- Fatuzzo, M., Adams, F.C., Gauvin, R., & Proszkow, E.M. 2006, PASP, 118, 1510
- Forget, F., & Pierrehumbert, R. T. 1997, Science, 278, 1273
- Fowles, Grant R., & Cassiday, George L., Analytical Mechanics 7th ed., Belmont, California, Thomson Brooks/Cole, Inc 2005
- Franck, S., von Bloh, W., Bounama, C., Steffen, M., Schönberner, D., & Schellnhuber, H. J., 2002, Astrobiology The Quest for the conditions of life., Berlin, Springer
- Freund, John E., 1999, Mathematical Statistics 6th ed., Upper Saddle River, New Jersey, Prentice-Hall, Inc.

- Garcia, Alejandro L., 2000, Numerical Methods for Physics 2nd ed., Upper Saddle River, New Jersey, Prentice-Hall, Inc.
- Gehman, C. S., Adams, F. C., & Laughlin, G. 1996, PASP, 108, 1018
- Gray, D. F. 1992, The Observation and Analysis of Stellar Photospheres, Cambridge University Press, Cambridge
- Hamilton, D. P., & Burns, J. A. 1992, Icarus, 96, 43
- Jones, B. W. 2008, Int. J. Astrobiology, 7, 279
- Jones, B. W., Sleep, P. N., & Chambers, J. E. 2001, A&A, 366, 254
- Jones, B. W., & Sleep, P. N., 2002 A&A, 393, 1015
- Jones, B. W., Underwood, D. R., & Sleep, P. N. 2005, ApJ, 622, 1091
- Jones, H. R. A., Butler, R. P., Tinney, C. G., Marcy, G. W., Carter, B. D., Penny, A. J., McCarthy, C., & Bailey, J. 2006, Mon. Not. R. Astron. Soc. 369, 249
- Kasting, J. F., Whitmire, D. P., & Reynolds, R. T. 1993, Icarus, 101, 108
- Koch, David, & Gould, Alan. Kepler Mission: A search for habitable planets, 2009.
<http://kepler.nasa.gov>
- Marcy, G. W., & Butler, R. P. 1998, ARA&A, 36, 57
- Marcy, G., Butler, R. P., Fischer, D., Vogt, S., Wright, J. T., Tinney, C. G., & Jones, H. R. A. 2005, Prog. Theor. Phys. Suppl., 158, 24
- Marcy, G., Butler, R. P., Vogt, S., Fischer, D. A., Henry, G. W., Laughlin, G., Wright, J. T., & Johnson, J. A. 2005, ApJ, 619, 570
- Marcy, G., Butler, R. P., Vogt, S. S., Fischer, D. A., Wright, J. T., Johnson, J. A., Tinney, C. G., Jones, H. R. A., Carter, B. D., Bailey, J., O'Toole, S. J., & Upadhyay, S. 2008, Physica Scripta, T130, 014001
- Menou, K., & Tabachnik, S. 2003, ApJ, 583, 473
- Mischna, M. A., Kasting, J. F., Pavlov, A., & Freedman, R. 2000, Icarus, 145, 546
- Murray, C. D., & Dermott, S. F., 2008, Solar System Dynamics, New York, New York, Cambridge University Press

- Noble, M., Musielak, Z. E., & Cuntz, M. 2002, *ApJ*, 572, 1024
- Pillai, S. U., Li, K. Y., & Himed, B., 2007, *Space Based Radar: Theory and App.*,
New York City, New York, McGraw-Hill Professional
- Press, W. H., Flannery, B. P., Teukolsky, S. A., & Vetterling, W. T. 1989, *Numerical Recipes, The Art of Scientific Computing*, Cambridge Univ. Press, New York
- Sándor, Zs., Sűli, Á., Érdi, B., Pilat-Lohinger, E., Dvorak, R. 2007, *MNRAS*, 375, 1495
- Schneider, Jean, *The Extrasolar Planets Encyclopedia*, 2009,
<http://www.exoplanet.eu>
- Spiegel, D. S., Menou, K., & Scharf, C. A. 2008, *ApJ*, 681, 1609
- Stix, M., *The Sun 2nd ed.*, 2004, New York, New York, Springer, Inc.
- Turnbull, M. C., & Tarter, J. C. 2003, *ApJS*, 145, 181
- Underwood, D. R., Jones, B. W., & Sleep, P. N. 2003, *Int. J. Astrobiology*, 2, 289
- Unwin, S. C., et al. 2008, *PASP*, 120, 38
- Valenti, J. A., & Fischer, D. A. 2005, *ApJS*, 159, 141
- von Bloh, W., Cuntz, M., Franck, S., & Bounama, C. 2003, *Astrobiology*, 3, 681
- von Bloh, W., Bounama, C., & Franch, S. 2003, *Clest. Mech. & Dyn. Astro.*, 92, 287
- von Bloh, W., Bounama, C., & Franck, S. 2007, *Planet. Space Sci.*, 55, 651

BIOGRAPHICAL STATEMENT

Katherine Elizabeth Yeager was born in Hamilton, Ohio, in 1985. She received her B.S. in Physics from Wright State University, in 2007, and her M.S. in Physics from The University of Texas at Arlington in 2009. She became interested in astronomy at a very early age and developed a love for physics during her senior year of high school. It was combining these two passions that she decided to pursue a Master's in Physics with an emphasis in astrophysical research. Katherine became interested in orbital mechanics and astrobiology while at UTA and hopes to be able to incorporate these interests in future research projects.